

PRESUPERNOVA EVOLUTION WITH IMPROVED RATES FOR WEAK INTERACTIONS

A. HEGER, S. E. WOOSLEY, G. MARTÍNEZ-PINEDO, AND K. LANGANKE

Department of Astronomy and Astrophysics
University of California, Santa Cruz, CA 95064

Institut for Fysik og Astronomi
Århus Universitet, DK-8000 Århus C, Denmark
Submitted ApJ, 27 November 2000

ABSTRACT

Recent shell-model calculations of weak-interaction rates for nuclei in the mass range $A = 45 - 65$ have resulted in substantial revisions to the hitherto standard set of Fuller, Fowler, & Newman (FFN). In particular, key electron-capture rates, such as that for ^{60}Co are much smaller. We consider here the effects of these revised rates on the presupernova (post-oxygen burning) evolution of massive stars in the mass range 11 to $40 M_{\odot}$. Moreover, we include, for the first time in models by our group, the effects of modern rates for beta-decay in addition to electron capture and positron emission. Stars of 15, 25, and $40 M_{\odot}$ stars are examined in detail using both the full FFN rate set and the revised rates. An additional finely spaced (in mass) grid of 34 models is also calculated in order to give the systematics of iron core and silicon core masses. Values for the central electron mole number at the time of iron core collapse in the new models are typically larger, by $\Delta Y_e = 0.005$ to 0.015 , than those of Woosley & Weaver (1995), with a tendency for the more massive models to display larger differences. About half of this change is a consequence of including beta-decay; the other half, result of the smaller rates for electron capture. Unlike what might be expected solely on basis of the larger Y_e 's, the new iron core masses are systematically smaller owing to a decrease in the entropy in the outer iron core. The changes in iron core mass range from zero to $0.1 M_{\odot}$ (larger changes for high mass stars). It would be erroneous though to estimate the facility of exploding these new models based solely upon their iron core mass since the entire core structure is altered and the density change is not so different as the adjustments in composition might suggest. We also observe, as predicted by Aufderheide *et al.* (1994a), a tendency towards beta-equilibrium just prior to the collapse of the core, and the subsequent loss of that equilibrium as core collapse proceeds. This tendency is more pronounced in the $15 M_{\odot}$ model than in the heavier stars. We discuss the key weak reaction rates, both beta-decay and electron-capture, responsible for the evolution of Y_e and make suggestions for future measurements.

Subject headings: stars: supernovae, nucleosynthesis

1. INTRODUCTION

The effect of weak interactions on the final evolution of massive stars is known to be quite pronounced (e.g., Weaver, Woosley, & Fuller 1984). Weak interactions alter the composition and change the nucleosynthesis. They modify the structure of the iron core and its overlying mantle and thus help to determine whether the star explodes and the characteristics of the bound remnant. Electron capture decreases the number of electrons available for pressure support and, all else being equal, decreases the effective Chandrasekhar Mass that can be supported without collapsing. Beta decay acts in the opposite direction. Weak interactions also create neutrinos that, for all densities until the collapse becomes truly hydrodynamic (i.e., $\rho \lesssim 10^{11} \text{ g cm}^{-3}$), escape the star carrying away energy and thereby reducing entropy. In fact, for stars that are not too massive, neutrinos from weak interactions, as opposed to thermal plasma processes, are the dominant energy sink in the presupernova star (Weaver, Zimmerman, & Woosley 1978). Reducing the entropy also makes the iron core smaller (Timmes, Woosley, & Weaver 1996).

Over the years, many people have calculated weak interaction rates for astrophysical application (Hansen 1966, 1968; Mazurek 1973; Mazurek *et al.* 1974; Takahashi, Yamada, & Kondo 1973; Aufderheide *et al.* 1994b). For approximately 15 years though, the standard in the field has been the tabulations

of Fuller, Fowler, & Newman (1980, 1982a,b, 1985) (henceforth FFN). These authors calculated rates for electron capture, beta-decay, and positron emission, plus the associated neutrino losses for all astrophysically relevant nuclei ranging in atomic mass from 23 to 60. Their calculations were based upon an examination of all available information (in the mid 1980's) for individual ground states and low-lying excited states in the nuclei of interest. Recognizing that this only saturated a small part of the Gamow-Teller resonance, they extrapolated the known experimental rates using a simple (single-state) representation of this resonance.

Now, as we briefly summarize in Sect. 2, new shell models of the distribution of Gamow-Teller strength have resulted in an improved - and often reduced - estimate of its strength. The alteration in some important rates, such as electron capture on ^{60}Co , is as large as two orders of magnitude in important astrophysical circumstances. In order to determine how these new rates affect the post-oxygen burning evolution of massive stars and presupernova models, we have examined the evolution of a fine grid of 34 stellar models spanning a mass range 11 to $40 M_{\odot}$. The post-oxygen burning evolution of each star was calculated twice - once using the same old set of weak rates as employed in Woosley & Weaver (1995) (henceforth WW) by Tom Weaver in 1996 (priv. com.; unpublished) and, again, with the new rates. It is important to note that the models of WW in-

cluded electron capture and positron decay rates from FFN, but used beta-decay rates from Hansen and Mazurek. These were much smaller than their FFN counterparts and essentially resulted in beta decay being neglected. This was a mistake, that, so far as we are aware, was not replicated in the more recent works of other groups (Thielemann, Nomoto, & Hashimoto 1996; Chieffi, Limongi, & Straniero 1998). An examination of conditions in the pre-supernova model led to the (correct) conclusion that beta-decay was negligible there. What was overlooked however, as was subsequently pointed out (Aufderheide *et al.* 1994a), was the importance of beta-decay in the iron core a few hours *before* iron core collapse.

The new weak rate implementation described here *does* include beta-decay - along with revised rates for electron capture and positron emission. In order to make a fair comparison to what would have been obtained by WW had they used the full FFN implementation, we have recalculated (Sect. 3) three stars (15, 25, and 40 M_{\odot}) using FFN beta decay rates as well as FFN electron-capture and positron-decay rates keeping the stellar physics (thermal neutrino loss rates, opacities, mass loss, etc.) the same as in WW. Subsequent survey of massive stellar evolution (Rauscher *et al.* 2000; Heger *et al.* 2001) will implement the full revised weak rate set along with many other improvements in a fine grid of masses and metallicities.

We find (Sect. 4) significant differences in the presupernova models calculated using the new rates. In particular, the large decrease in key rates for electron-capture and the inclusion of beta-decay result in an electron mole number, Y_e , in the center of the presupernova star that is 1% to 4% larger. Changes around 3% are most common and there is a tendency for the biggest changes to occur for larger stellar masses. The altered weak rates also affect the structure of the presupernova star, leading to iron core masses that are, almost without exception, *smaller*. This seemingly paradoxical result (smaller Fe core and larger Y_e) comes about because of a decreased entropy in the outer iron core, a consequence of a final stage of silicon shell burning.

In Sect. 6 we summarize our findings and enumerate key rates that warrant further laboratory study (see also Tables 1–6).

2. THE NEW RATES

Weak interactions in presupernova stars are known to be dominated by allowed Fermi and Gamow-Teller transitions (Bethe *et al.* 1979). FFN estimated their rates based upon the presence of a single Gamow-Teller (GT) resonance which they derived on the basis of the independent particle model, supplemented, where available, by experimental data for low-lying transitions. However, recent experimental data on the GT distributions in nuclei (Alford *et al.* 1990; Vetterli *et al.* 1989; Alford *et al.* 1993; El-Kateb *et al.* 1994; Williams *et al.* 1995) shows a quenching of the total GT strength compared to the independent-particle model value. More importantly, the data also show a fragmentation of the GT strength over many states in the daughter nucleus. Due to the strong dependence of the phase space on the energy, particularly for stellar electron capture, an improved treatment of the relevant nuclear structure is called for (Aufderheide *et al.* 1993a,b).

The origin of the quenching and fragmentation of the GT strength distribution has been traced to nucleon-nucleon correlations, in particular, correlations between protons and neutrons. Furthermore, studies of *sd*-shell nuclei ($A = 17–39$) by Brown & Wildenthal (1988) have shown that reproduction of

the observed GT strength distributions requires the inclusion of all nucleon-nucleon correlations within the complete shell. This requires the shell model. Following the work by Brown and Wildenthal, Oda *et al.* (1994) calculated shell-model rates for all the relevant weak processes for *sd*-shell nuclei. Complete shell model calculations for the heavier *pf*-shell nuclei were deferred because these require model spaces orders of magnitude larger. Such calculations only became possible after significant progress both in shell-model programming and computer power.

Today, shell-model calculations for the *pf*-shell can be performed at a truncation level which guarantees convergence. Caurier *et al.* (1999), in particular, have demonstrated that state-of-the-art diagonalization studies, typically involving a few times 10 million configurations, can reproduce all the relevant ingredients - the GT_{\pm} strength distributions for changing protons (neutrons) into neutrons (protons), the level spectra, and the half lives - and hence have the predictive power to calculate accurate stellar weak interaction rates for nuclei up to $A = 65$. A survey of the *pf*-shell nuclei has been completed by Langanke & Martínez-Pinedo (2000) and is ready for incorporation in stellar models. In this paper we combine the rate sets of Oda *et al.* (up to $A = 40$) with those of Langanke and Martínez-Pinedo for $A = 45$ to 65. Shell-model rates for nuclei with $A = 40–44$ are not yet available, as these nuclei require the inclusion of both *sd*- and *pf*-shells. In our studies we have used the FFN rates for these nuclei. We shall refer to the hybrid collection as the “LMP rate set”. Though it clearly involves multiple sources, the most important, uncertain rates for the late stages of stellar evolution involve the *pf*-nuclei. Though these new shell-model rates and the FFN rates agree rather well for *sd*-shell nuclei (Oda *et al.* 1994), there are appreciable differences at higher mass. The electron-capture rates, and to a lesser extent, the β -decay rates (see Martínez-Pinedo, Langanke, & Dean 2000) are smaller than the FFN rates by, on average, one order of magnitude. The causes have been discussed by Langanke & Martínez-Pinedo (2000).

We include in our studies rates for electron and positron captures and β^+ and β^- decays. Energy losses by neutrinos, and hence core cooling, are determined from the (tabulated) average neutrino energies which have been consistently calculated from the shell-model studies for each of the weak processes. In addition to the rates themselves, the energy losses to neutrinos can have an important effect on the stellar structure, particularly in the post-silicon burning phase (neutrino losses *during* silicon burning are dominated by thermally produced neutrinos). Fig. 1 shows the mean neutrino energies emitted during electron capture on various parent nuclei using the LMP and FFN tabulations. There is considerable variation in the ratio, but a significant tendency for the neutrinos emitted by weak interactions in the post-silicon burning phase (e.g., $T_9 = 5$) to have higher mean energies in the LMP rate set.

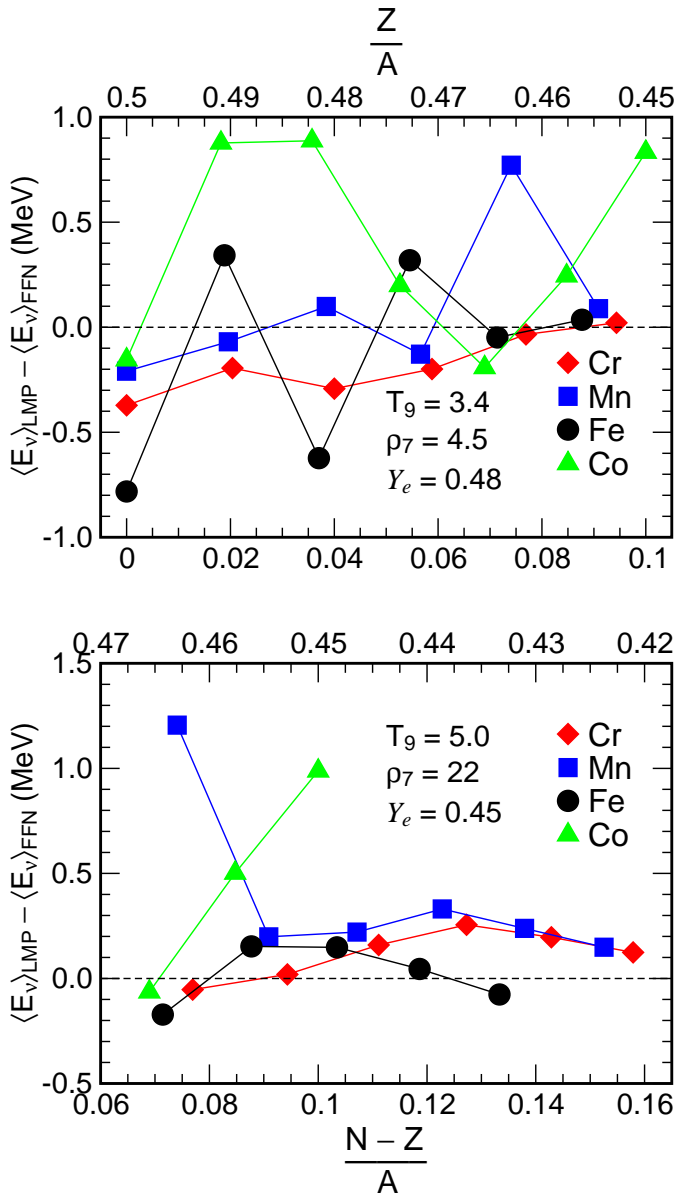


FIG. 1.— Differences between the average neutrino energies emitted during electron capture for the new calculations of LMP and the old ones of FFN for several isotopic chains. The upper panel reflects the conditions during silicon core burning while the lower panel reflects the conditions during core contraction. In general, though not universally, the neutrino energies are larger in the new rate set. The entropy and energy losses associated with a certain amount of electron capture will thus be greater in the new models.

3. STELLAR MODELS

All models were calculated using a modified version of the KEPLER implicit hydrodynamics code (Weaver *et al.* 1978). In order to facilitate comparisons with earlier work, recent improvements to the code – the inclusion of OPAL opacities, mass loss, rotationally induced mixing, and recent revisions to nuclear reaction rates (other than weak rates) were not included. A total of 34 models were calculated. The procedure and models were as close as we could manage to WW. Pre-explosive hydrogen, helium, carbon, and neon burning and the early stages of central oxygen burning should not be affected by the current revision of the weak rates and so all studies commenced from previously existing “binary restart dumps” that were made when the central oxygen abundance was depleted, by oxygen

burning, to a mass fraction $X(^{16}\text{O}) = 0.04$. The evolution was then followed through the remainder of oxygen burning, silicon core and shell burning, and the early stages of collapse. The “presupernova model” was defined as the time when the collapse velocity near the edge of the iron core first reached 1000 km s^{-1} , as in Woosley & Weaver (1995). In the remainder of the paper we refer to this time as t_0 .

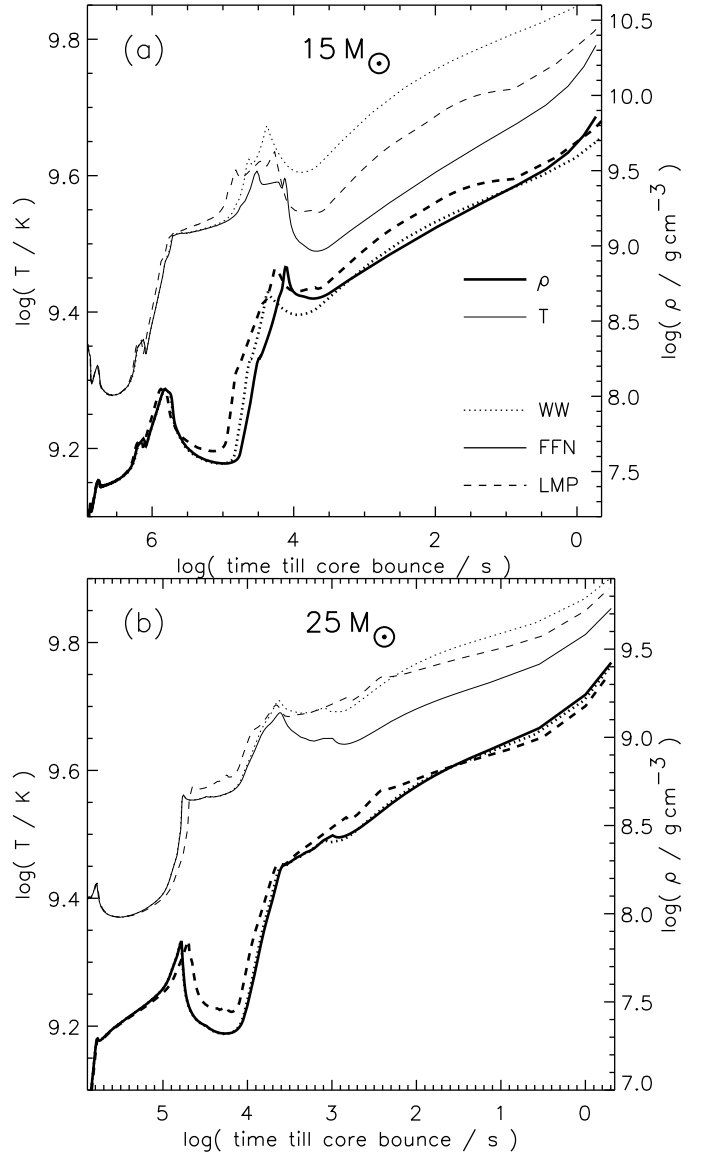


FIG. 2.— Histories of the central temperature (*thin lines*) and density (*thick lines*) in 15 and $25 M_{\odot}$ presupernova stars calculated using the rate set of Woosley & Weaver (1995) (WW; *dotted lines*), the full implementation of FFN rates (electron capture and beta decay; *solid lines*) and the new weak interaction rates of Langanke & Martínez-Pinedo (LMP; *dashed lines*).

Three versions of KEPLER were employed. One was the same as in WW and was used to duplicate the earlier calculations in order to obtain additional edit quantities for comparison. The second used the new rate set described in Sect. 2. These included rates for electron capture, beta decay, and positron emission from (Langanke & Martínez-Pinedo 2000) (henceforth LMP) for nuclei heavier than mass 45 and from Oda *et al.* (1994) and FFN for nuclei lighter than mass 45, as explained above. We shall find that it is the nuclei above mass

45 that determine Y_e and the presupernova structure. The effects of positron capture were estimated to be small for the stars under consideration here (though not perhaps for much more massive stars) and were *not* included in our calculations. In order to preserve accuracy using a table with a limited number of temperature and density points, an effective ft value was determined for the electron capture rates by dividing out the first order dependence on Fermi integrals (this was also done with the FFN rates in prior work by WW). The rates for beta decay and positron emission, however, were interpolated logarithmically (using a cubic spline) in the tables provided. The mean energy of neutrinos emitted in each reaction are also given by LMP, Oda *et al.*, and FFN. These were also interpolated logarithmically. A third version of KEPLER was the same as WW except for the incorporation of FFN beta decay. Where results are given in this paper labelled “FFN”, they refer to calculations using this third version of KEPLER. Similarly, “LMP” refers to the second and “WW” to the first.

All three versions were used to study 15, 25, and 40 M_\odot presupernova models and these are the three stars that will be used for illustration in this paper. The presupernova models from these calculations are available to those wishing to study their further (explosive) evolution. An additional set of 31 other masses were also studied in the 11 - 40 M_\odot range. Details of these models, calculated by Tom Weaver in 1995 and 1996, remain unpublished though they were discussed and used in Timmes *et al.* (1996) and employed identical physics to those in WW. Oxygen depletion dumps were available for these stars and a second version of the presupernova evolution of each was calculated using the LMP rates. The comparison of results for these additional models will be useful later in the paper where systematics of core entropy, iron core mass, silicon core mass, and Y_e are discussed.

Fig. 2 shows the evolution of the 15 and 25 M_\odot models using the WW rates (WW), the FFN rates (FFN), and the new weak rates (LMP) and defines the temperature-density region of interest in this study. The time axis in this and subsequent figures warrants some explanation. WW defined “presupernova”, somewhat arbitrarily, as that point in the final evolution of a massive star when any point in its iron core reached a collapse velocity in excess of 1000 km s^{-1} . Operationally, this was a good time to link the results of a stellar evolution model to a calculation of the explosion mechanism since the codes used to study the explosion could usually only follow dynamic evolution. Another fiducial time is that instant, which we shall call the “bounce time”, t_b , when the iron core collapses to supra-nuclear density and rebounds creating a shock wave. This might be more properly regarded as the end of the star’s life and the beginning of the supernova. We estimated t_b by running the KEPLER calculation until the central density exceeded $10^{12} \text{ g cm}^{-3}$. This is within a millisecond or so of the core bounce. We used this estimate of t_b in all our graphs and tables. Because of the accelerating evolution of the star, evolving quantities are best plotted against the logarithm of the time remaining until t_b .

4. RESULTS AND DISCUSSION

Tables 1 – 3 summarize some interesting physical quantities at representative times in the fiducial set of 15, 25, and 40 M_\odot stars. Though three sets of models (WW, FFN, and LMP) were studied, only two are included in the tables. As we shall see, beta decay remains unimportant until where after the depletion of silicon in the center of the star. Thus the results labeled FFN

are equivalent to WW until the star reaches silicon shell burning. Afterwards, it is more meaningful to compare results using the new rate LMP set to what would have been obtained using an equivalent full implementation of the FFN rates than comparing to the calculations of WW.

The times chosen for edit in Tables 1 – 3 are somewhat arbitrary but attempt to capture the essence of the evolutionary state of the center of the star at equal times before core bounce and at times representative of oxygen depletion (“O-dep”); oxygen shell burning (“O-shell”); the ignition of silicon in the core (first convection; “Si-ign”); half-way through silicon burning (“Si-dep”); the end of convective core silicon burning (“Si-dep”); the ignition of the first stage of convective silicon shell burning (“Si-shell”); after silicon shell extinction (“core contr”); and the presupernova star as defined in Sect. 3. In Tables 1 – 3, the relation between “presupernova” time and t_b , the core bounce time, is clearly stated.

In addition to the values of the central temperature, density, and Y_e , key energy generation and loss terms, entropies, and weak flows are also edited. The specific central nuclear energy generation rates, the weak and plasma neutrino losses and the total energy “generation” rate is given next. Then we give the total central entropy and its contributions by electrons, ions, radiation and pairs, and in the next two lines the proton mole fraction and the rate of electron capture onto protons. The last row before the horizontal line gives the total net weak rate. Below that line we give first the five most important ions that *decrease* Y_e (electron capture and β^+ -decay) and their rates (below the ion symbol) and then sum up the total rates of electron capture and β^+ -decay. In the last part of the table we first give the five most important nuclei that *increase* Y_e (positron capture and β^- -decay) and in the last line the total rate of β^- -decay.

For comparison to the “pre-SN” values given in Tables 1 – 3 for the FFN and LMP rate sets, we note that the central entropies at the equivalent times using the WW models were 0.73, 0.97, and 1.10 for the 15, 25, and 40 M_\odot models respectively.

From these tables, one can infer many of the alterations that come about as a consequence of the new rate set. However, there are a few we want to emphasize.

4.1. The evolution of Y_e and the approach to beta equilibrium

Fig. 3, Fig. 4, and Fig. 5 show the evolution of the central value of Y_e for different choices of rate set. For the 15 M_\odot model, which as we shall see briefly achieves full dynamic beta-equilibrium, the choice of rate set is not so important as the inclusion of beta-decay. The old results of WW are essentially a lower bound to the Y_e one expects when beta decay is zero. For the higher mass stars, the actual size of the electron capture rates has a more significant effect amounting to about half of the difference between the WW models and the new models.

Most of the change in central Y_e in the 15 M_\odot models occurs during the period 10^6 to 10^4 s before core collapse. This is a time (Table 1) when the star is either burning silicon in its core ($\log(t_b - t) = 5.8$ to 4.8) or is resting in hydrostatic equilibrium with a central core of iron while silicon burns in a shell at about 1.1 M_\odot . Capture rates on iron group nuclei are thus most important. It is also interesting that the final Y_e is set to within a percent or so well *before* the iron core begins its final Kelvin-Helmholtz contraction (the last hour). This means that the most important period for determining core structure, or at least the electron fraction in the center, occurs, not during the dynamic implosion of the star, but during silicon shell burning.

Table 1 also shows the importance of neutrino losses from

weak interactions during these final stages. For the $15 M_{\odot}$ model, neutrino losses from electron capture and beta-decay exceed thermal neutrino losses *in the center of the star* during and after silicon shell burning (but not in the shell itself). By the time of the presupernova model, neutrino losses from weak flows are over four orders of magnitude greater in the center of the star than those from thermal neutrinos. They are also competing with photodisintegration in causing the collapse of the core.

For the 25 and $40 M_{\odot}$ models, the situation is similar though thermal neutrinos are more important at later times and constitute about 1% of the central energy loss rate in the presupernova star.

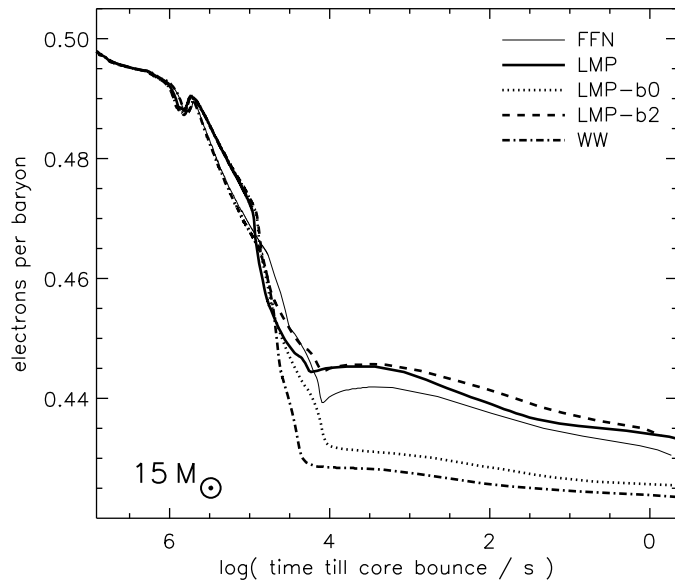


FIG. 3.— Evolution of Y_e with time at the center of five $15 M_{\odot}$ stars that used a) the new rates (LMP; dark solid line); b) the full implementation of FFN rates including beta-decay (light solid line); and c) the weak rates used by WW (dot-dashed line). Also shown for comparison are the results using the LMP rates with beta-decay rates multiplied by zero and two. The WW models are very similar to what is obtained when beta-decay is neglected. The final central values of Y_e for the models are in case a) 0.432; b) 0.430; and c) 0.423 (Table 1).

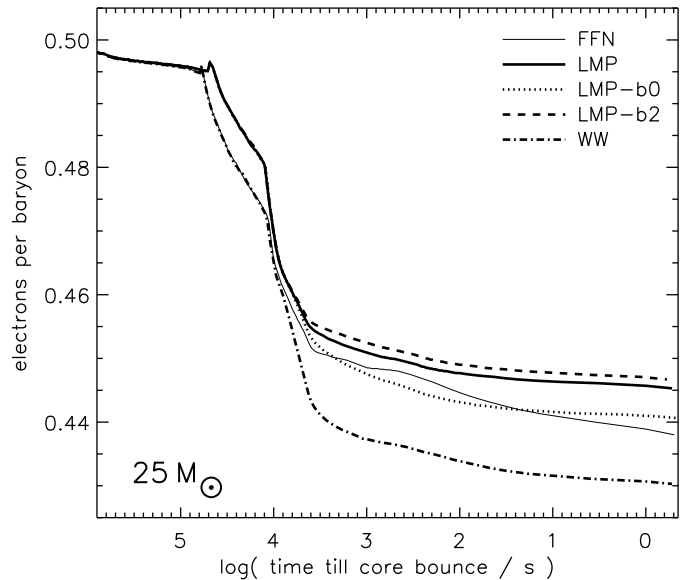


FIG. 4.— Same as Fig. 3, but for $25 M_{\odot}$ models. Here the revised rates for electron capture and the inclusion of beta decay have comparable effects on the central evolution. The final central values of Y_e for the models are in case a) 0.445 for LMP rates; b) 0.438 for FFN rates; and c) 0.430 for the WW model.

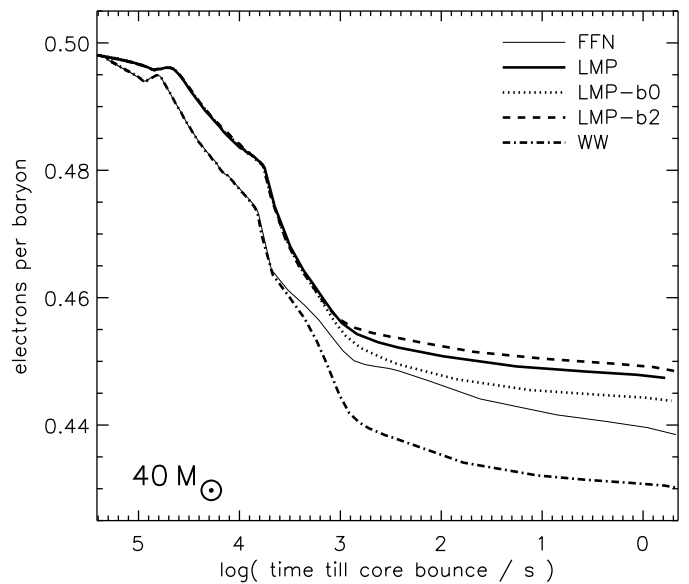


FIG. 5.— Same as Fig. 3, but for $40 M_{\odot}$ models. As for the $25 M_{\odot}$ star (Fig. 4), the revised rates for electron capture and the inclusion of beta decay have comparable effects on the central evolution. The final central values of Y_e for the models are a) 0.447 for LMP rates, b) 0.439 for FFN rates, and c) 0.430 for the WW models.

An interesting phenomenon observed in all models that included modern rates for beta-decay was the approach, during the late stages of silicon shell burning and early iron core contraction, to dynamic beta-equilibrium (Tables 1 – Table 3; Fig. 6, and Fig. 7). Such a close approach was not observed in models using the older rates (Fig. 6). About 1 to 10 hours prior to core collapse in the $15 M_{\odot}$ model, for example, the total rate of beta-decay very nearly balances the total rate of electron capture. Such a balance, as foreseen by Aufderheide *et al.* (1994a), is never quite achieved, with the new rates, in the 25 and $40 M_{\odot}$ models, though it comes closer with the rates of

FFN. It is important to note that this state of *dynamic* equilibrium is not the same as true weak equilibrium (such as exists in the early instants of the Big Bang). A state of detailed balance does *not* exist between all URCA pairs. The gas is still transparent to neutrinos and the reciprocal processes of electron capture and beta decay, i.e., neutrino capture and anti-neutrino capture, are quite negligible. This makes it impossible to assign a local chemical potential to the neutrinos. Moreover, electron capture on a given nucleus, A_Z , including all states, ground and excited, does not occur at a rate very nearly equal to the beta decay of ${}^A_{(Z-1)}$. Rather it is the integral of all beta decays that balances a similar integral of all electron captures to render dY_e/dt close to zero and Y_e stationary. Of course, evolution does occur as the temperature and density evolve, and eventually this dynamic beta-equilibrium ceases to exist. “Freeze-out” happens as the density rises to the point that electron capture is favored, but the rates become too slow to maintain steady state.

Another feature of this dynamic equilibrium that distinguishes it from true equilibrium is that the rates still matter. The abundances are not, in general, given simply by the Saha equation. A systematic decrease in electron capture rates, for example, shifts the steady state Y_e at a given temperature and density to a larger value. However, the change is not great. A larger Y_e implies a greater abundance of nuclei that are less neutron-rich and whose beta-decay rates will be smaller because of the lower Q -values. The distribution responds by decreasing Y_e to the point where, globally, electron capture again balances beta decay. A similar “restoring force” occurs if Y_e is displaced to smaller values. Since the Q -values enter as high powers in the phase space integrals, there is, overall, a *nearly* unique solution for Y_e at a given temperature and density. This explains, in part, the robust value of the final Y_e in the $15 M_\odot$ model. Though the important electron capture rates are, at a given temperature, density, and Y_e , quite a bit smaller in the new models, a small adjustment of Y_e in steady state compensates for this so that the final value of Y_e doesn’t change much. In the 25 and $40 M_\odot$ models where dynamic beta equilibrium is not achieved, Y_e remains more sensitive to the rates.

Despite the fact that electron capture flows are not, in general, balanced by beta decay for each pair of nuclei, there are some interesting URCA pairs apparent in Tables 1 – 3. For example, during silicon shell burning and core contraction in the $15 M_\odot$ star (Table 1), ${}^{57}\text{Fe}(e^-, \nu){}^{57}\text{Mn}$ and ${}^{56}\text{Fe}(e^-, \nu){}^{56}\text{Mn}$ are two of the three most important electron capture flows, but ${}^{57}\text{Mn}(e^-\bar{\nu}){}^{57}\text{Fe}$ and ${}^{56}\text{Mn}(e^-\bar{\nu}){}^{56}\text{Fe}$ are also two of the three most important beta-decay flows. The rates for these forward and inverse reactions are calculated independently, but perhaps there is some approach to weak equilibrium in progress. The so called “back resonances” in beta decay proceed through the same Gamow-Teller resonance that dominates in electron capture.

Not every reaction is so balanced though. The flow due to ${}^{61}\text{Co}(e^-\bar{\nu}){}^{61}\text{Ni}$ at the same conditions is about twelve times smaller than that from ${}^{61}\text{Ni}(e^-, \nu){}^{61}\text{Co}$.

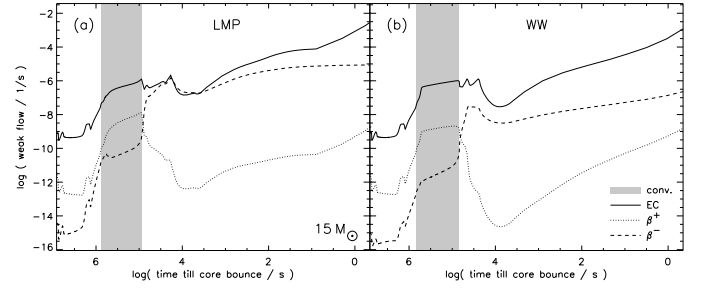


FIG. 6.— Partial contributions to the evolution of the central electron mole number, Y_e , as a function of time until dynamic collapse in a $15 M_\odot$ star. The calculation on the left used the new LMP rates. A calculation using the full implementation of the FFN rates would look very similar. Note the initial dominance of electron capture, but a period around $\log(t_b - t) = 3.5$ to 4.5 when beta-decay balances electron capture. Still later, the increasing density in the contracting core favors electron capture again and beta-decay cannot keep up. However, time has become so short that Y_e changes very little in these last few hours (Fig. 3). The right hand figure shows the calculation of WW where beta equilibrium was not achieved. The shaded region is the epoch of convective silicon core burning.

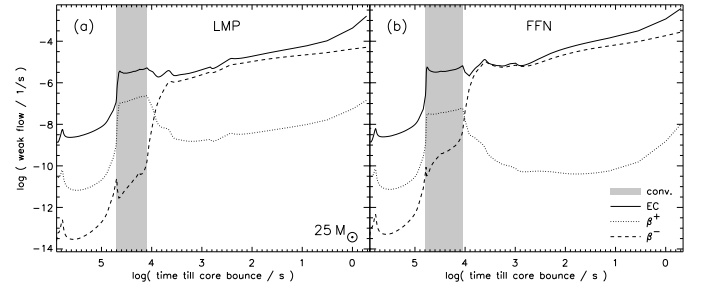


FIG. 7.— Same as Fig. 6, but for $25 M_\odot$ models and the comparison is with respect to the full FFN implementation rather than WW. Using the new LMP rates, beta-decay competes with electron-capture, but never quite balances it. Using FFN rates, beta equilibrium is achieved. A plot for the $40 M_\odot$ models is very similar. A plot of the calculation using the WW rates resembles Fig. 6. The shaded region is the epoch of convective silicon core burning.

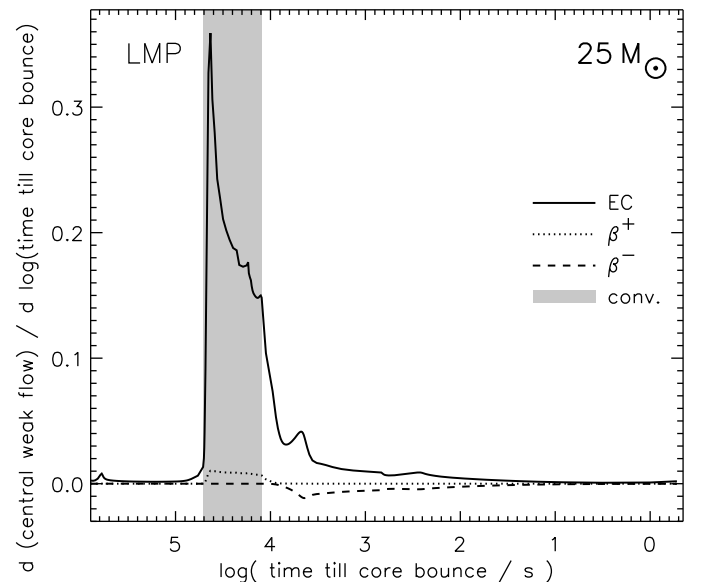


FIG. 8.— Time-weighted weak flows in the $25 M_\odot$ model using the weak rates of LMP. Most of the change in Y_e is consequence of electron capture though beta decay becomes important at late times.

4.2. Sensitivity to Beta-Rates and Network

Because of the state of near beta-equilibrium, the actual value of the beta-decay rates does not greatly matter, so long as they are large enough to instigate the equilibrium. Calculations in which all beta-decay rates are arbitrarily multiplied by factors of 2 and 5 give very similar results to those in which the standard values are used (Fig. 3 and Fig. 4; plots with beta-decay rates times 5, omitted for clarity in those figures, are very similar to those where the rates were multiplied by 2). However, if the beta rates become sufficiently small (approximated by zero here), the evolution is greatly altered and the results with the new rates resemble more closely what was obtained in the WW models.

One might be concerned about the relative sparsity of the reaction network used here to calculate abundances in nuclear equilibrium, 125 isotopes. This network, very similar to that used by Weaver *et al.* (1978), is reasonably complete up to nickel, but contains no heavier isotopes. It contains 67 iron-group species including $^{44-52}\text{Ti}$, $^{47-54}\text{V}$, $^{48-56}\text{Cr}$, $^{51-58}\text{Mn}$, $^{52-62}\text{Fe}$, $^{54-64}\text{Co}$, and $^{56-66}\text{Ni}$. Studies by Aufderheide *et al.* (1994b), using a much larger network, suggest that this group of isotopes should be adequate to represent both electron capture and beta decay for $Y_e \gtrsim 0.43$ (see their Tables 16, 17, 22, and 23). The larger values of Y_e we now obtain for presupernova stars (Tables 1 – 3) mean that the current network is more applicable. However, we are concerned that the isotopes contributing most to beta decay in the presupernova model frequently lie on the neutron-rich boundary of our network. We intend to expand its size to include both more neutron-rich isotopes in the iron group and more flows above Ni in the near future.

4.3. Important individual weak rates

By far the most important electron-capture rate in calculations that use the FFN rates is $^{60}\text{Co}(e^-, \nu)^{60}\text{Fe}$. This dominates the evolution of Y_e in the center of the star from silicon depletion onwards. This particular rate is greatly reduced in the new LMP rate set (Langanke & Martínez-Pinedo 1999), and this is one of the main reasons Y_e is larger in the cores of the new stars (Tables 1 – 6; Figs. 9 and 10).

In the new models using LMP rates, several electron capture reactions dominate (Tables 1 – 3). Even capture on free protons is no longer negligible, particularly in more massive stars at late times (Figs. 9 and 10).

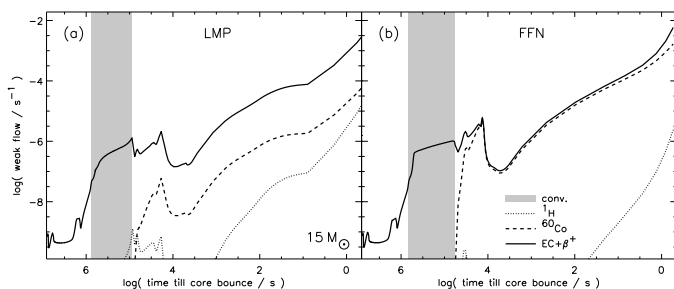


FIG. 9.— Major contributions to the electron capture flow for two $15 M_{\odot}$ stars that used the LMP rates (left) and the FFN rates (right). For the FFN rates, the evolution after $\log(t_0 - t) = 5$ is dominated by electron capture on ^{60}Co . Electron capture is unimportant. For the LMP rates, electron capture on ^{60}Co is unimportant, but capture on free protons is beginning to contribute in the presupernova model, a trend that will probably continue as the star collapses. During the pre-collapse evolution though, most of the flow in the LMP models is carried by electron-capture on other heavy nuclei, especially $^{54,55,56,57}\text{Fe}$, ^{55}Mn , and ^{61}Ni (Table 1). The shaded region is the epoch of convective silicon core burning.

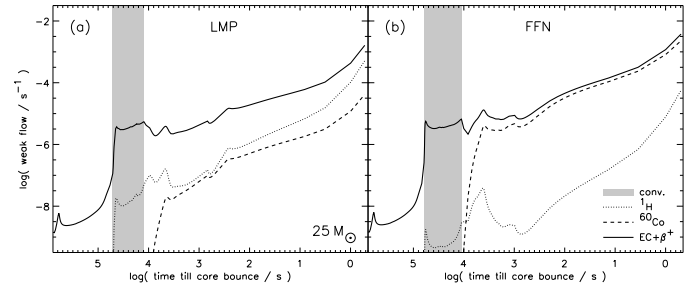


FIG. 10.— Major contributions to the electron capture flow for two $25 M_{\odot}$ stars that used the LMP rates (left) and the FFN rates (right). See also Fig. 9. Again the evolution of Y_e in the model using the FFN rates is almost completely determined by $^{60}\text{Co}(e^-, \nu)^{60}\text{Fe}$. The evolution of the model with LMP rates on the other hand is determined by other nuclei, especially $^{53,54,55,56}\text{Fe}$, ^{55}Co and ^{56}Ni (Table 2) with an increasingly important contribution from electron capture on free protons. A graph for the $40 M_{\odot}$ model looks similar, except that at collapse $p(e^-, \nu)n$ contributes almost the entire flow. The shaded region is the epoch of convective silicon core burning.

5. CHANGES IN THE PRESUPERNOVA STRUCTURE

The structure of the presupernova star is altered both by the changes in Y_e and entropy in its deep interior. The altered composition and entropy also affect the location and extension of convective shells and can cause changes in structure that extend outside the region where the rates themselves were altered. For some masses of star that may have been on the verge of discontinuous behavior, e.g., igniting an additional convective shell of silicon or oxygen burning, such changes can be quite dramatic.

The general behavior of the density structure and iron core mass in terms of electronic entropy per baryon, S_e , and Y_e can be understood in terms of the definition of the Chandrasekhar mass generalized for finite temperature (Chandrasekhar 1938; Timmes *et al.* 1996, e.g.)

$$M_{\text{Ch}} \simeq 5.83 Y_e^2 \left[1 + \left(\frac{S_e}{\pi Y_e} \right)^2 \right]. \quad (1)$$

Here S_e is expressed in units of Boltzmann's constant, k_B , and is dimensionless. Note that, under circumstances in massive stars, the entropy can be just as important as Y_e in determining the effective Chandrasekhar Mass.

The practical difficulty applying this equation is that both Y_e and S_e vary with the location in the core. Figs. 11 and 12 show the composition, density, $Y_e(m)$, $S_e(m)$, and total entropy $S_{\text{tot}}(m)$ in the cores of 15 and $25 M_{\odot}$ stars.

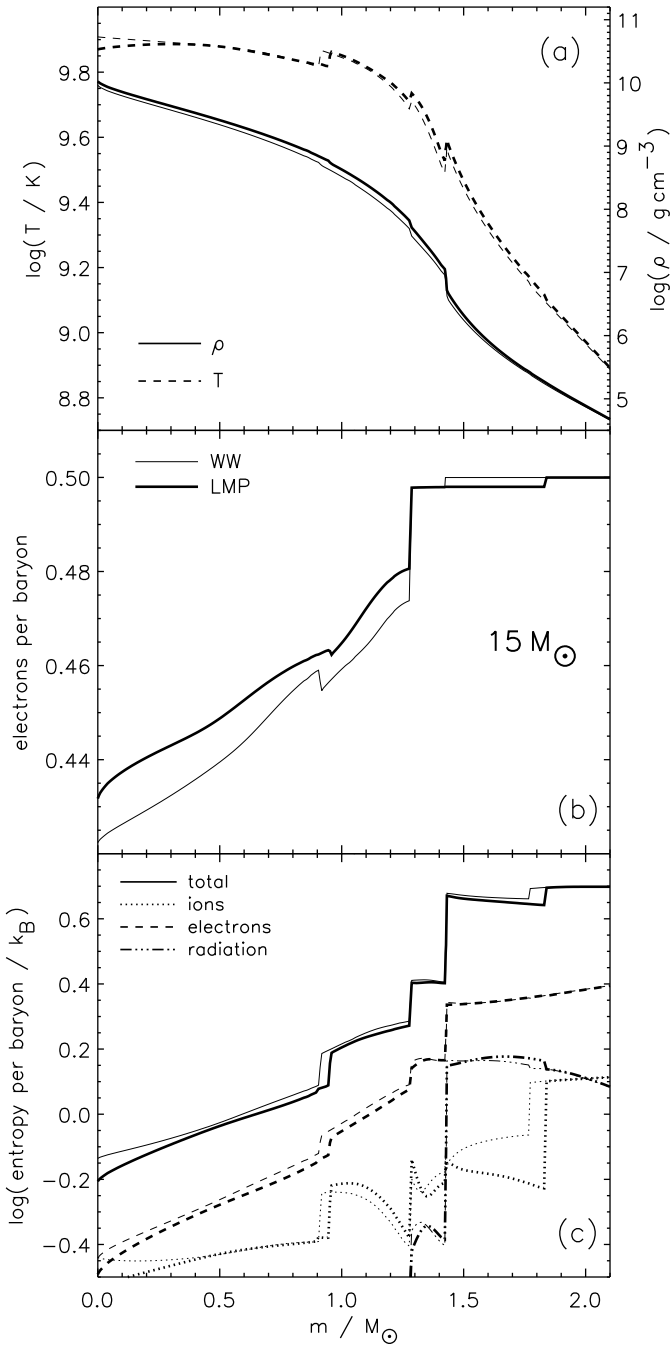


FIG. 11.— Structure of the $15 M_{\odot}$ presupernova star as calculated by WW and recalculated using the new LMP rates. Note the lower central entropy in the LMP model. The discontinuities in T , Y_e , and entropy at $0.98 M_{\odot}$ in the LMP model and $0.92 M_{\odot}$ in the WW model show the extent of the first stage of silicon core burning. In the FFN model (not shown) this discontinuity is located at $0.98 M_{\odot}$. The abrupt increase in Y_e at $1.29 M_{\odot}$ in all three models marks the maximum extent of the silicon convective shell and the edge of the iron core. The total entropy and its components are shown. The LMP rates give a lower entropy both in the center and outer core. The entropy jump at $1.43 M_{\odot}$ in all the models is the location of the oxygen burning shell (edge of the silicon core).

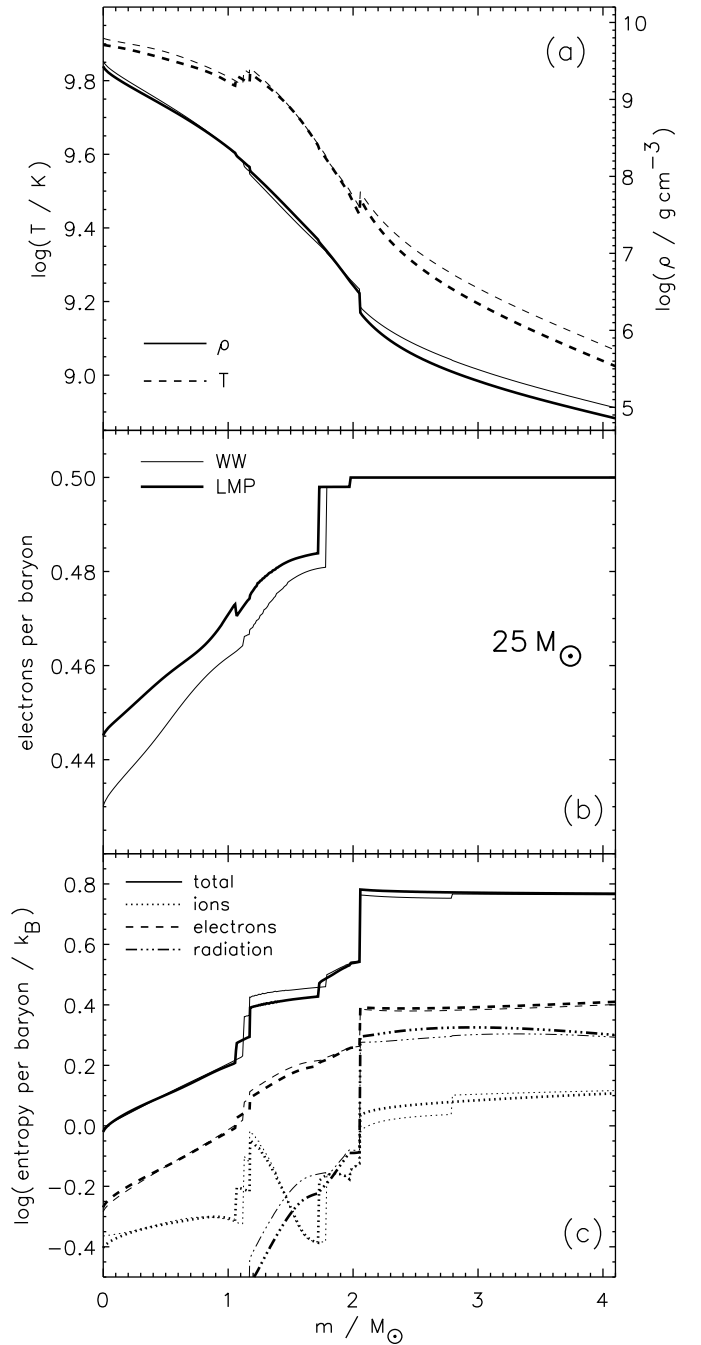


FIG. 12.— Structure of the $25 M_{\odot}$ presupernova. Similar to Fig. 11, but the decrease in central entropy for the LMP based model is less pronounced. The central entropy for the FFN model (not shown) is smaller than either of these. The maximum extent of the silicon convective core gives fossil discontinuities in T , Y_e , and the entropy at $1.07 M_{\odot}$ in the LMP model, $1.12 M_{\odot}$ in the WW models, and $1.18 M_{\odot}$ in the FFN model. The jump in Y_e at $1.72 M_{\odot}$ in the LMP model and $1.78 M_{\odot}$ in both the WW and FFN models marks the maximum extent of the silicon convective shell and the edge of the iron core. The jump in entropy at $2.06 M_{\odot}$ in all three models is the base of the oxygen shell (i.e., the edge of the silicon core).

A second difficulty is that the “iron core” and the core one compares to the Chandrasekhar mass are not necessarily the same. Typically, unless there is explosive burning during the collapse, the outer boundary of the iron core marks the final extension of the last stage of silicon shell burning. There is usually a discontinuous jump of entropy at that point and a consequent fall off in density. This makes the iron core a meaningful parameter in the calculation of the explosion mechanism. However, this jump in entropy is not nearly so large as the one associated with the very vigorous oxygen burning shell at the outer edge of the silicon shell. Thus the iron core is only approximately isolated from the overlying material. Its surface boundary pressure is often not negligible.

Still, several general tendencies are evident. First, $Y_e(m)$ is larger for the new rates *everywhere* in all the new cores. This must act to increase the mass of the compact core (and the iron core within) when it collapses. However, the entropy profile also shows significant changes. As Fig. 14 shows, the central entropy is *lower* for the new models (LMP) compared with old ones (WW) for stellar masses up to about $27 M_\odot$, and there is a tendency, at least at low mass, for the decrease in entropy to correlate inversely with the mass. Inclusion of beta-decay, which was left out by WW, leads to weak equilibrium in the centers of stars in this mass range (Sect. 4.1; Figs. 6 and 7) and the accompanying extra neutrino losses from this URCA-like process gives a decreased entropy. This decrease in entropy helps to offset the increase in Y_e in determining the iron core mass. However, above about $27 M_\odot$ the central entropies are *higher*. Full beta equilibrium is not achieved in these stars (using the LMP rates) and the neutrino cooling that would have accompanied such equilibrium is decreased. Moreover, there is less electron capture with the new rates, and less neutrino cooling by this process as well, so the entropy is higher. If central entropy were all that mattered, the larger Y_e in these big stars would imply larger iron cores, contrary to what is observed (Fig. 13).

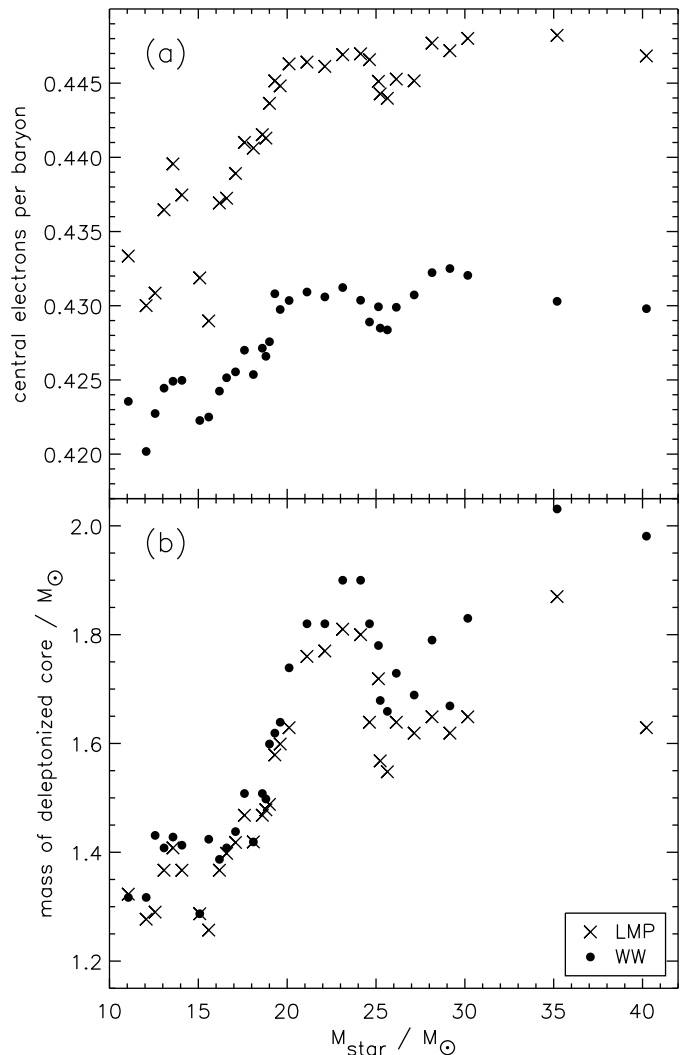


FIG. 13.— Central values of Y_e (a) and masses of the “deleptonized core” (b) at the time of iron core implosion for a finely spaced grid of stellar masses. The “deleptonized core” mass is defined as the mass interior to the point where the Y_e is 0.49. Despite the larger values of Y_e for the new rates (Panel a), the deleptonized core masses are not changed very much for the most common variety of supernovae, those with masses below $20 M_\odot$. However larger changes result for stars of higher mass.

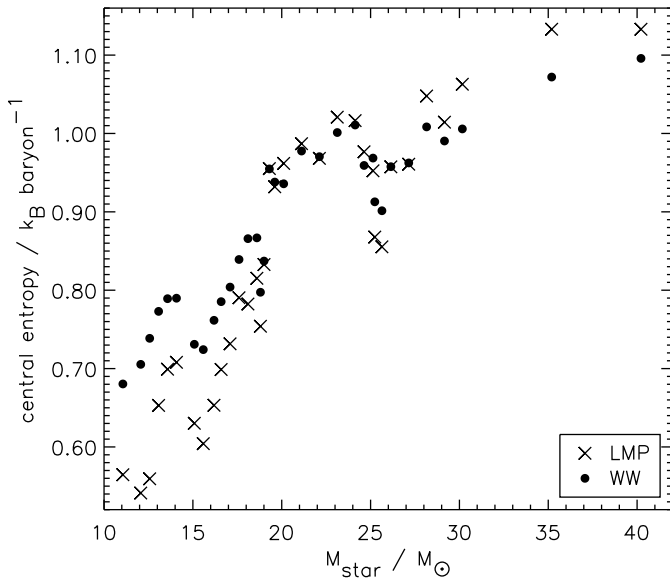


FIG. 14.— Total entropy at the center of a collection of presupernova stars of varying mass. Crosses indicate models calculated with the new weak rates (LMP); circles use the rate set of WW. For stellar masses below about $20 M_{\odot}$ the entropy is systematically lower in the new models. From 20 to $27 M_{\odot}$ the entropy is not changed very much, though there are exceptions at 25 and $26 M_{\odot}$. Above $27 M_{\odot}$, the trend seen at lower masses reverses itself and the new models have higher total central entropy. However to see the effect of entropy on the iron core mass, one must really consider the distribution of electronic entropy in the entire iron core (Figs. 11 and 12).

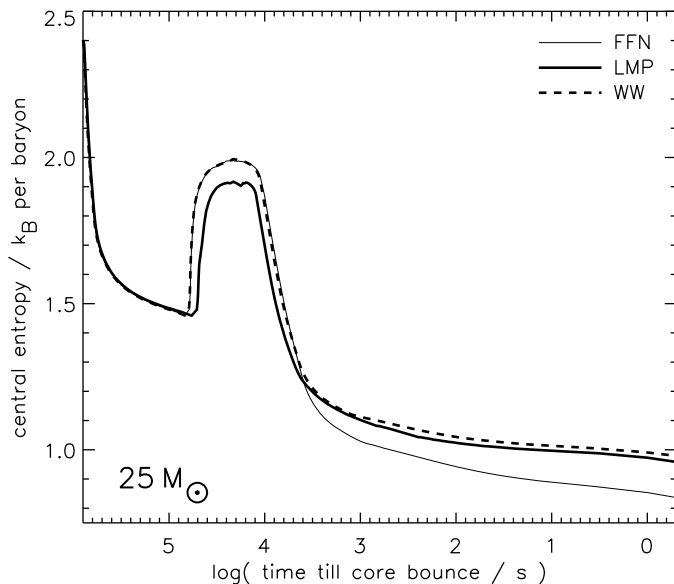


FIG. 15.— Evolution of the central entropy in $25 M_{\odot}$ models using weak rates from FFN, LMP, and WW. The bump starting at $\log(t_0 - t) = 4.7$ is due to core silicon burning (Fig. 2). In general, the advanced stages of nuclear burning in the cores of massive stars cause rises in entropy followed by declines as neutrinos cool the depleted region while shell burning supports the star. The model of WW tracks the FFN curve until beta decay becomes important, then coincidentally follows the LMP trajectory. At late times, the entropy using the full FFN rate set is lower because continued beta equilibrium leads to additional cooling (Fig. 7).

This seeming paradox results because conditions in the outer core are more important to determining the final distribution of composition than those in the inner core. None of our stars collapse following the first stage of silicon core burning. All have

one or more stages during which silicon burns in a convective shell around an inert iron core. It is the extent of these convective shells that determines the boundary between iron- and silicon-rich compositions in the pre-supernova star. The extent of these convective shells is sensitive to the entropy in the surrounding material, the entropy developed in the convective shell, and its composition.

For convection according to the Ledoux criterion, as used in KEPLER, the change in Y_e between two zones affects the criteria for mixing. It is more difficult to mix two regions if the Y_e of the underlying material is smaller. However, the difference is not great and it actually acts in the opposite direction to what is observed. That is, the smaller Y_e in the FFN models should make the growth of the convective shell more difficult and the iron core smaller. Clearly another effect is at work - the entropy itself.

The entropy in the convective silicon shell (and during silicon core burning; Tables 1 – 3) is smaller with the new rates (Figs. 11 and 12). During silicon burning, beta decay has not yet become important (Figs. 6 and 7). Differences that arise in the silicon shell between the old WW models and the new ones are thus solely a consequence of the altered rates for and neutrino losses associated with electron capture and not effected by the neglect, by WW, of beta decay. The larger value of entropy obtained with the old rates is partly a consequence of increased energy generation during silicon burning (Tables 1 – 3, see “Si core burning”). Lowering Y_e (i.e., using the FFN rates) means that silicon burns to nuclei in the iron group that are more tightly bound. ^{56}Fe is more tightly bound than ^{54}Fe which is, in turn, more tightly bound than ^{56}Ni . Neutronization also brings into play more efficient channels of silicon destruction. For Y_e near 0.50, silicon burns at a rate set by $^{24}\text{Mg}(\gamma, \alpha)^{20}\text{Ne}$ (Bodansky, Clayton, & Fowler 1968). For Y_e appreciably below 0.50 though, $^{26}\text{Mg}(p, \alpha)^{23}\text{Na}$ becomes an efficient alternative using ^{26}Mg that is in quasi-equilibrium with $^{28,29,30}\text{Si}$. Consequently, silicon burning is a little briefer and yields a little more energy per gram with the FFN rates. Because of the higher specific energy, it can burn at a lower temperature. Because of this and the shorter duration, there are less neutrino losses to pair processes. The mean neutrino energies are also larger when one captures on nuclei that are abundant at larger Y_e . For all these reasons, the entropy associated with silicon burning is a little bit less with the new rates.

The effects on the iron core mass can be cumulative. Because the entropy of the first stage of convective core burning is less (Fig. 15), the $25 M_{\odot}$ star ends up igniting its silicon shell at $1.07 M_{\odot}$ instead of $1.12 M_{\odot}$ (Fig. 12). This puts the silicon shell deeper in the “entropy well” to begin with. Then the entropy of shell burning is also lower. Combining these effects leads to the silicon convective shell not extending as far as it did with the old rates. Because the entropy gradients, and the consequent barrier to the growth of the convective shell, are shallower in more massive stars, the change in the iron core mass is larger there.

5.1. Implications for the Explosion Mechanism and Neutron Star Masses

Despite the emphasis placed upon differences in Y_e and entropy in the previous section, the most striking feature of the density plots in Fig. 11 and Fig. 12 is their similarity. The appreciable changes in iron core mass are not really accompanied by large changes in the core structure. The location of the large entropy jump associated with the oxygen burning shell

also does not change (Fig. 16). Still, the success or failure of explosion calculations often hinges on small differences in the accretion rate, radius of the stalled shock, and neutrino luminosity (e.g., Janka 2000). One may expect revisions, if only in the net explosion energy. These revisions cannot be anticipated in advance because they rely on the highly non-linear outcome of a system where more than one key parameter is being varied.

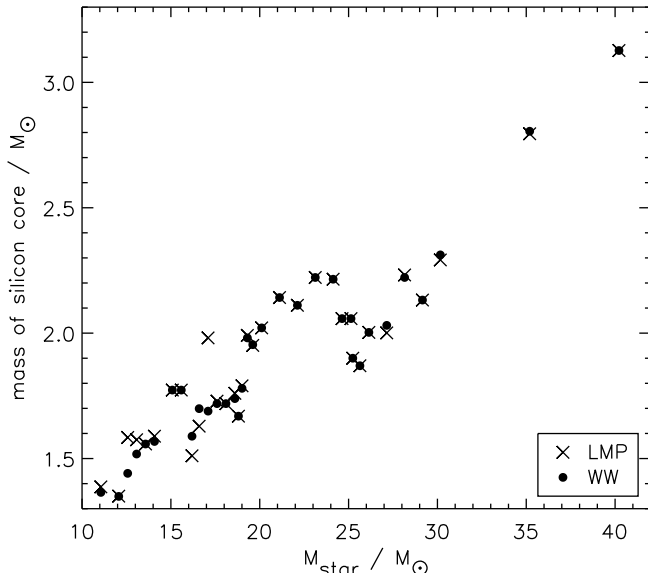


FIG. 16.— Silicon cores for the two sets of weak rates. The silicon core is defined as the point where the oxygen abundance declines to very small values. Typically there is a large entropy jump associated with the base of the oxygen shell so that the silicon core may be as relevant for the explosion mechanism as the iron core mass. The weak rates do not have a great effect on the mass of the silicon core.

Generally speaking, iron cores with larger Y_e and smaller mass are easier to explode. The larger Y_e implies a larger “homologous core” and the prompt shock is born farther out with less overburden (Bethe 1990). A smaller iron core also decreases the losses the shock experiences to photodisintegration before breaking free. But it is very doubtful that the new models are so different as to allow “prompt” hydrodynamic explosions. That being the case, the density just outside the iron core is also very important as that sets the “ram pressure” that any neutrino-powered explosion must overcome. The density in this region is larger in the new models by as much as 50%. So, in the neutrino powered models, currently favored, the new models could actually be more difficult to explode.

6. CONCLUSIONS

We have explored in some detail the weak interactions that characterize the last few days in the life of a massive star. In particular we have studied the effects of a new, improved set of weak interaction rates and neutrino losses by Langanke & Martínez-Pinedo (2000) and the role played by beta-decay as well as electron capture.

In agreement with Aufderheide *et al.* (1994a), we find that inclusion of beta decay makes a significant difference in the presupernova structure. Beta equilibrium comes to exist, temporarily, in the center of the star after silicon is depleted. This causes the final electron mole number, Y_e , to be larger than in models where beta decay has been neglected (e.g., Woosley & Weaver 1995). The existence of beta equilibrium, particularly

in the lower mass stars ($M \lesssim 20 M_\odot$), also decreases the central entropy. Both effects alter the structure of the presupernova star.

In addition to the consequences of including beta decay, we find that which rate set one uses also makes a difference. In particular, for the more massive stars studied here, use of the new weak rates of LMP instead of the older set from FFN causes an additional increase in Y_e comparable to that from the inclusion of beta decay. This is because the new rates for electron capture are systematically smaller owing to a more accurate treatment of the Gamow-Teller resonance. All in all, Y_e in the iron cores of the new models is systematically larger by approximately 3% (Fig. 13). Since Y_e enters quadratically into determining the Chandrasekhar Mass and since the mass of the iron core is critically important in models for the supernova explosion mechanism, this is a significant difference.

However, contrary to simple expectations based only upon the change in Y_e , the new iron core masses are systematically about 0.05 to 0.1 M_\odot smaller than in WW (Fig. 13). This has several causes, but chiefly reflects the lower entropy in the convective silicon shell just prior to iron core collapse. The lower entropy inhibits the final growth of the iron core in a surrounding medium of fixed entropy.

In total, the new presupernova models may explode more easily due both to their reduced iron core mass and larger Y_e , however the changes are not large and there are other effects (lower entropy just outside the iron core) that could act in the opposite direction. The new 15, 20, and 25 M_\odot models discussed here are available to those wanting to study the explosion mechanism.

As Tables 1 – 6 show, some of the most interesting weak processes in presupernova stars involve unstable, radioactive nuclei for which no experimental data exists about the GT strength distribution. This situation should change once the proposed Rare-Isotope Accelerator (RIA) and similar facilities become operational. These accelerators will allow studies of the GT distributions in unstable nuclei by charge-changing reactions like ($d, ^2\text{He}$) or ($^{12}\text{C}, ^{12}\text{N}$) in inverse kinematics. Such experiments, as well as high-precision beta-decay measurements will either verify or severely constrain the nuclear models. They will also determine energies, quantum numbers, and low-lying transition strengths at low excitation energies.

For example, the shell model calculations predict that, with increasing neutron excess, the centroid of the GT distribution moves to lower excitation energies in the daughter nucleus (Langanke & Martínez-Pinedo 2000 see Fig. 8 in). It would be very helpful to quantify this prediction experimentally. Such data could appreciably improve our understanding of proton-neutron correlations and of the evolution of the $f_{7/2} - f_{5/2}$ spin-orbit splitting in the pf -shell.

There are also currently no experimental data regarding the GT_+ distribution for odd-odd nuclei in the pf -shell. This is particularly unfortunate given the key role played by capture on ^{60}Co in the FFN rates. The shell model electron capture rates for odd-odd nuclei, however, are significantly – often by more than one order of magnitude at the relevant temperature and density – lower than the FFN estimates and this is largely responsible for the difference between the FFN and LMP presupernova models. This is because the shell model places the centroid of the GT strength distribution for odd-odd nuclei at noticeably higher excitation energies in the daughter nucleus.

We are grateful to Rob Hoffman, for help in implement-

ing the different versions of the weak rates into the KEPLER code, and to Tom Weaver for providing the stellar models starting at oxygen depletion that were used for the finely binned (in mass) study of stellar models and the presupernova models that used the input physics of WW. This work was supported by the National Science Foundation (AST-97-31569 and AST-

INT-9909999), by the ASCI Program of the U.S. Department of Energy by under contract No. W-7405-Eng-48, by the Alexander von Humboldt-Stiftung (FLF-1065004), and by the Danish Research Council. GMP was supported by the Carlsberg Foundation.

REFERENCES

- Alford, W. P., Helmer, R. L., Abegg, R., Celler, A., Frekers, D., Green, P., Haeusser, O., Henderson, K., Hicks, K., Jackson, K. P., Jeppesen, R., Miller, C. A., Trudel, A., Vetterli, M., Yen, S., Pourang, H., Watson, J., Brown, B. A., & Engel, J. 1990, *Nucl. Phys.*, A514, 49
- Alford, W. P., Brown, B. A., Burzynski, S., Celler, A., Frekers, D., Helmer, R., Henderson, R., Jackson, J. P., Lee, K., Rahav, A., Trudel, A., & Vetterli, M. 1993, *Phys. Rev.*, C48, 2818
- Aufderheide, M. B., Bloom, S. D., Ressler, D. A., & Mathews, G. J., 1993a, *Phys. Rev.*, C47, 2961
- Aufderheide, M. B., Bloom, S. D., Ressler, D. A., & Mathews, G. J., 1993b, *Phys. Rev.*, C48, 1677
- Aufderheide, M. B., Fushiki, I., Fuller, G. M., & Weaver, T. A. 1994a, *ApJ*, 424, 257
- Aufderheide, M. B., Fushiki, I., Woosley, S. E., & Hartmann, D. H. 1994b, *ApJS*, 91, 389
- Aufderheide, M. B., Bloom, S. D., Mathews, G. J., Resler D. A. 1996, *Phys. Rev.*, C53, 3139
- Bethe, H. A. 1990, *Rev Mod Phys.* 62, 801
- Bethe, H. A., Brown, G. E., Applegate, J. M., and Lattimer, J. M. 1979, *Nuc. Phys. A.*, 324, 487
- Bodansky, D., Clayton, D. D., & Fowler, W. A. 1968, *ApJS*, 16, 299
- Brown, B. A., & Wildenthal, B. H. 1988, *Ann. Rev. Nucl. Part. Sci.*, 38, 29
- Caurier, E., Langanke, K., Martínez-Pinedo, G., & Nowacki, F. 1999, *Nucl. Phys.*, A653, 439
- Chieffi, A., Limongi, M., & Straniero, O. 1998, *ApJ*, 502, 737
- Chandrasekhar, S. 1938, *An Introduction to the Study of Stellar Structure*, University of Chicago Press, reissued 1957 by Dover Press
- El-Kateb, S., Jackson, J.P., Alford, W.P., Abegg, R., Azuma, R.E., Brown, B.A., Celler, A., Frekers, D., Haeusser, O., Helmer, R., Henderson, R.S., Hicks, K.H., Jeppesen, R., King, J.D., Raywood, K., Shute, G.G., Spicer, B.M., Trudel, A., Vetterli, M. & Yen, S. 1994, *Phys. Rev.*, C49, 3128
- Fuller, G. M., Fowler, W. A., & Newman, M. J. 1980, *ApJS*, 42, 447
- Fuller, G. M., Fowler, W. A., & Newman, M. J. 1982a, *ApJS*, 48, 279
- Fuller, G. M., Fowler, W. A., & Newman, M. J. 1982b, *ApJ*, 252, 715
- Fuller, G. M., Fowler, W. A., & Newman, M. J. 1985, *ApJ*, 293, 1
- Hansen, C. J., 1966, PhD Thesis, Yale Univ.
- Hansen, C. J. 1968, *Ap&SS*, 1, 499
- Heger, A., Hoffman, R. D., Rauscher, T., & Woosley, S. E. 2000, in *Nuclear Astrophysics, Ringberg Proceedings X*, in press and in preparation for *ApJ*, astro-ph-0006350
- Herant, M., Benz, W., Hix, W.R., Fryer, C. L., Colgate, S. A. 1994, *ApJ*, 435, 339
- Janka, T. 2000, *A&A*, in press, see also astro-ph/0008432.
- Langanke, K. & Martínez-Pinedo, G. 1999, *Phys. Lett. B.*, 453, 187
- Langanke, K., & Martínez-Pinedo, G. 2000, *Nucl. Phys. A.* 673, 481
- Martínez-Pinedo, G., Langanke, K. & Dean, D. J. 2000, *ApJS*, 126, 493
- Mazurek, T. 1973, PhD Thesis, Yeshiva Univ.
- Mazurek, T., Truran, J. W., & Cameron, A. G. W. 1974, *Ap&SS*, 27, 261
- Oda, T., Hino, M., Muto, K., Takahara, M., & Sato, K. 1994, *Atomic Data & Nucl. Data Tables*, 56, 231
- Rauscher, T., Heger, A., Woosley, S. E., & Hoffman, R. D. 2000, to be submitted to *ApJ*
- Takahashi, K., Yamada, M., & Kondo, T. 1973, *ADNDT*, 12, 101
- Thielemann, F.-K., Nomoto, K., & Hashimoto, M. 1996, *ApJ*, 460, 408
- Timmes, F. X., Woosley, S. E., & Weaver, T. A. 1996, *ApJ*, 457, 834
- Vetterli, M., Haeusser, O., Abegg, R., Alford, W.P., Celler, A., Frekers, D., Helmer, R., Henderson, R., Hicks, K.H., Jackson, J.P., Jeppesen, R.G., Miller, C.A., Raywood, K. & Yen, S. 1989, *Phys. Rev.*, C40, 559
- Weaver, T. A., Woosley, S. E., & Fuller, G. M. 1984, in *Numerical Astrophysics*, eds. J. Centrella, J. LeBlanc and R. Bowers (Jones and Bartlett), p. 374
- Weaver, T. A., Zimmerman, G. B., & Woosley, S. E. 1978, *ApJ*, 225, 1021
- Williams, A.L., Alford, W.P., Brash, E., Brown, B.A., Burzynski, S., Fortune, H.T., Haeusser, O., Helmer, R., Henderson, R., Hui, P.P., Jackson, J.P., Larson, B., MacKinzie, M.G., Smith, D.A., Trudel, A., & Vetterli, M. 1990, *Phys. Rev.*, C51, 1144
- Woosley, S. E., & Weaver, T. A. 1995, *ApJS*, 101, 181

TABLE 1
 PROPERTIES OF THE STELLAR CENTER OF A 15 M_⊙ STAR

	O-dep		O-shell		Si-ign		Si-burn	
	FFN	LMP	FFN	LMP	FFN	LMP	FFN	LMP
$\log(t_b - t)$	6.91	6.91	6.51	6.51	5.84	5.90	5.30	5.30
T	$2.26 \cdot 10^9$	$2.26 \cdot 10^9$	$1.90 \cdot 10^9$	$1.90 \cdot 10^9$	$2.87 \cdot 10^9$	$2.86 \cdot 10^9$	$3.32 \cdot 10^9$	$3.39 \cdot 10^9$
ρ	$1.23 \cdot 10^7$	$1.24 \cdot 10^7$	$2.74 \cdot 10^7$	$2.75 \cdot 10^7$	$1.09 \cdot 10^8$	$1.08 \cdot 10^8$	$3.88 \cdot 10^7$	$4.46 \cdot 10^7$
Y_e	$4.98 \cdot 10^{-1}$	$4.98 \cdot 10^{-1}$	$4.95 \cdot 10^{-1}$	$4.95 \cdot 10^{-1}$	$4.89 \cdot 10^{-1}$	$4.89 \cdot 10^{-1}$	$4.76 \cdot 10^{-1}$	$4.80 \cdot 10^{-1}$
ϵ_{nuc}	$9.63 \cdot 10^{10}$	$9.24 \cdot 10^{10}$	$1.01 \cdot 10^9$	$1.01 \cdot 10^9$	$1.36 \cdot 10^{11}$	$1.08 \cdot 10^{11}$	$3.28 \cdot 10^{13}$	$2.97 \cdot 10^{13}$
$\epsilon_{\nu, \text{weak}}$	$1.22 \cdot 10^9$	$1.19 \cdot 10^9$	$4.23 \cdot 10^8$	$4.21 \cdot 10^8$	$4.38 \cdot 10^{10}$	$3.92 \cdot 10^{10}$	$1.12 \cdot 10^{12}$	$9.08 \cdot 10^{11}$
$\epsilon_{\nu, \text{plas}}$	$1.52 \cdot 10^{11}$	$1.52 \cdot 10^{11}$	$3.76 \cdot 10^9$	$3.81 \cdot 10^9$	$6.49 \cdot 10^{10}$	$6.24 \cdot 10^{10}$	$2.45 \cdot 10^{12}$	$2.56 \cdot 10^{12}$
ϵ	$-5.74 \cdot 10^{10}$	$-6.10 \cdot 10^{10}$	$-3.18 \cdot 10^9$	$-3.21 \cdot 10^9$	$2.74 \cdot 10^{10}$	$6.13 \cdot 10^9$	$2.92 \cdot 10^{13}$	$2.62 \cdot 10^{13}$
S	1.78	1.78	1.34	1.34	1.25	1.25	1.57	1.52
S_e	1.03	1.03	$6.77 \cdot 10^{-1}$	$6.77 \cdot 10^{-1}$	$6.20 \cdot 10^{-1}$	$6.20 \cdot 10^{-1}$	$9.64 \cdot 10^{-1}$	$9.47 \cdot 10^{-1}$
S_{ion}	$6.35 \cdot 10^{-1}$	$6.36 \cdot 10^{-1}$	$6.28 \cdot 10^{-1}$	$6.28 \cdot 10^{-1}$	$6.02 \cdot 10^{-1}$	$6.03 \cdot 10^{-1}$	$4.88 \cdot 10^{-1}$	$4.68 \cdot 10^{-1}$
S_{rad}	$1.13 \cdot 10^{-1}$	$1.13 \cdot 10^{-1}$	$3.03 \cdot 10^{-2}$	$3.03 \cdot 10^{-2}$	$2.65 \cdot 10^{-2}$	$2.64 \cdot 10^{-2}$	$1.14 \cdot 10^{-1}$	$1.06 \cdot 10^{-1}$
S_{pair}	$7.55 \cdot 10^{-4}$	$7.53 \cdot 10^{-4}$	$1.11 \cdot 10^{-5}$	$1.11 \cdot 10^{-5}$	$1.76 \cdot 10^{-5}$	$1.72 \cdot 10^{-5}$	$1.69 \cdot 10^{-3}$	$1.43 \cdot 10^{-3}$
$Y(\text{p})$	$1.31 \cdot 10^{-13}$	$1.29 \cdot 10^{-13}$	$4.85 \cdot 10^{-17}$	$5.18 \cdot 10^{-17}$	$1.67 \cdot 10^{-12}$	$1.53 \cdot 10^{-12}$	$2.16 \cdot 10^{-9}$	$1.40 \cdot 10^{-8}$
$\lambda_{\text{p,tot}}$	$1.97 \cdot 10^{-17}$	$1.95 \cdot 10^{-17}$	$1.88 \cdot 10^{-20}$	$2.03 \cdot 10^{-20}$	$3.04 \cdot 10^{-14}$	$2.73 \cdot 10^{-14}$	$7.26 \cdot 10^{-12}$	$6.39 \cdot 10^{-11}$
λ_{weak}	$1.00 \cdot 10^{-9}$	$9.56 \cdot 10^{-10}$	$4.40 \cdot 10^{-10}$	$4.40 \cdot 10^{-10}$	$3.04 \cdot 10^{-8}$	$2.72 \cdot 10^{-8}$	$6.76 \cdot 10^{-7}$	$5.26 \cdot 10^{-7}$
$\lambda(\text{EC} + \beta^+)$	³⁵ Cl	³⁵ Cl	³⁵ Cl	³⁵ Cl	³³ S	³³ S	⁵³ Mn	⁵⁴ Fe
	$2.96 \cdot 10^{-10}$	$2.96 \cdot 10^{-10}$	$2.28 \cdot 10^{-10}$	$2.34 \cdot 10^{-10}$	$1.42 \cdot 10^{-8}$	$1.23 \cdot 10^{-8}$	$2.22 \cdot 10^{-7}$	$1.54 \cdot 10^{-7}$
	³⁷ Ar	³⁷ Ar	³³ S	³³ S	³⁵ Cl	³⁵ Cl	⁵⁵ Fe	⁵⁵ Fe
	$2.55 \cdot 10^{-10}$	$2.55 \cdot 10^{-10}$	$1.12 \cdot 10^{-10}$	$1.12 \cdot 10^{-10}$	$6.35 \cdot 10^{-9}$	$6.13 \cdot 10^{-9}$	$2.12 \cdot 10^{-7}$	$1.28 \cdot 10^{-7}$
	³² S	³² S	³⁷ Ar	³⁷ Ar	³¹ P	³¹ P	⁵⁴ Fe	⁵³ Mn
	$1.57 \cdot 10^{-10}$	$1.43 \cdot 10^{-10}$	$6.99 \cdot 10^{-11}$	$7.09 \cdot 10^{-11}$	$4.42 \cdot 10^{-9}$	$5.07 \cdot 10^{-9}$	$1.05 \cdot 10^{-7}$	$5.46 \cdot 10^{-8}$
	³⁶ Ar	³⁶ Ar	³² S	³² S	³² S	³² S	⁵⁷ Co	⁵⁰ Cr
	$1.06 \cdot 10^{-10}$	$1.23 \cdot 10^{-10}$	$1.25 \cdot 10^{-11}$	$1.21 \cdot 10^{-11}$	$2.74 \cdot 10^{-9}$	$2.23 \cdot 10^{-9}$	$3.31 \cdot 10^{-8}$	$3.86 \cdot 10^{-8}$
	³³ S	³³ S	³⁶ Ar	³⁶ Ar	³⁷ Ar	³⁷ Ar	⁵¹ Cr	⁵¹ Cr
	$9.90 \cdot 10^{-11}$	$9.55 \cdot 10^{-11}$	$5.08 \cdot 10^{-12}$	$4.82 \cdot 10^{-12}$	$7.51 \cdot 10^{-10}$	$6.67 \cdot 10^{-10}$	$2.52 \cdot 10^{-8}$	$3.20 \cdot 10^{-8}$
$\lambda_{\text{EC,tot}}$	$1.00 \cdot 10^{-9}$	$9.52 \cdot 10^{-10}$	$4.39 \cdot 10^{-10}$	$4.39 \cdot 10^{-10}$	$3.03 \cdot 10^{-8}$	$2.72 \cdot 10^{-8}$	$6.75 \cdot 10^{-7}$	$5.21 \cdot 10^{-7}$
$\lambda_{\beta^+, \text{tot}}$	$4.46 \cdot 10^{-12}$	$3.95 \cdot 10^{-12}$	$1.98 \cdot 10^{-13}$	$1.85 \cdot 10^{-13}$	$6.05 \cdot 10^{-11}$	$5.22 \cdot 10^{-11}$	$1.58 \cdot 10^{-9}$	$5.49 \cdot 10^{-9}$
$\lambda(\text{PC} + \beta^-)$	³² P	³² P	³² P	³² P	³² P	³² P	⁵⁵ Mn	⁵⁴ Mn
	$5.08 \cdot 10^{-15}$	$2.99 \cdot 10^{-15}$	$1.77 \cdot 10^{-15}$	$1.06 \cdot 10^{-15}$	$1.92 \cdot 10^{-11}$	$9.73 \cdot 10^{-12}$	$5.75 \cdot 10^{-10}$	$4.08 \cdot 10^{-11}$
	³⁶ Cl	³⁶ Cl	³⁶ Cl	³⁶ Cl	²⁸ Al	²⁸ Al	⁵³ Cr	⁵⁵ Mn
	$8.68 \cdot 10^{-16}$	$7.02 \cdot 10^{-16}$	$7.70 \cdot 10^{-17}$	$5.35 \cdot 10^{-17}$	$5.70 \cdot 10^{-13}$	$3.88 \cdot 10^{-13}$	$1.29 \cdot 10^{-10}$	$4.49 \cdot 10^{-12}$
	⁴⁶ Sc	⁴⁶ Sc	⁴⁶ Sc	⁴⁶ Sc	³³ P	³³ P	³² P	³² P
	$2.65 \cdot 10^{-16}$	$3.65 \cdot 10^{-17}$	$2.80 \cdot 10^{-17}$	$3.53 \cdot 10^{-18}$	$4.48 \cdot 10^{-13}$	$8.43 \cdot 10^{-14}$	$4.12 \cdot 10^{-11}$	$4.15 \cdot 10^{-12}$
	⁵⁵ Mn	⁵⁴ Mn	³³ P	⁵⁴ Mn	⁵⁵ Mn	⁵² V	⁵⁷ Fe	⁵⁸ Co
	$2.49 \cdot 10^{-17}$	$2.26 \cdot 10^{-17}$	$1.00 \cdot 10^{-17}$	$2.85 \cdot 10^{-18}$	$2.56 \cdot 10^{-13}$	$4.53 \cdot 10^{-14}$	$3.28 \cdot 10^{-11}$	$2.64 \cdot 10^{-12}$
	³³ P	³⁹ Ar	⁵⁵ Mn	³³ P	⁵³ Cr	³⁶ Cl	⁵⁴ Cr	⁵⁰ V
	$2.00 \cdot 10^{-17}$	$1.40 \cdot 10^{-17}$	$5.96 \cdot 10^{-18}$	$2.83 \cdot 10^{-18}$	$9.41 \cdot 10^{-14}$	$4.12 \cdot 10^{-14}$	$3.05 \cdot 10^{-11}$	$2.37 \cdot 10^{-12}$
$\lambda_{\beta^-, \text{tot}}$	$6.30 \cdot 10^{-15}$	$3.78 \cdot 10^{-15}$	$1.89 \cdot 10^{-15}$	$1.12 \cdot 10^{-15}$	$2.07 \cdot 10^{-11}$	$1.03 \cdot 10^{-11}$	$8.55 \cdot 10^{-10}$	$6.06 \cdot 10^{-11}$

NOTE.— For different stages of late stellar evolution (logarithm of time till core collapse, $t_b - t$ in s) we give for the FFN and LMP models the central values of temperature (T in K), density (ρ in g cm^{-3}), electrons per baryon (Y_e), specific energy generation rates: nuclear (ϵ_{nuc}), weak neutrino losses ($\epsilon_{\nu, \text{weak}}$), plasma neutrino losses ($\epsilon_{\nu, \text{plas}}$), and total (ϵ), all in $\text{erg g}^{-1} \text{s}^{-1}$, total entropy (S), electron entropy (S_e), ion entropy (S_{ion}), radiation entropy (S_{rad}) and entropy due to pairs (S_{pair}), all in k_B baryons $^{-1}$, the number fraction of protons ($Y(\text{p})$), the rate of electron captures on protons ($\lambda_{\text{p,tot}}$ in s^{-1}), and the total net weak rate ($\lambda_{\text{weak}} = dY_e/dt$ in s^{-1}). The different contribution to λ_{weak} are shown separately in the second section: we give the weak rates of the five most important isotopes for EC and β^+ -decay (upper part) and for PC and β^- -decay (lower part), and the total rates of EC ($\lambda_{\text{EC,tot}}$), β^+ -decay ($\lambda_{\beta^+, \text{tot}}$), and β^- -decay ($\lambda_{\beta^-, \text{tot}}$), all in s^{-1} per nucleon.

(CONTINUED ON NEXT PAGE)

TABLE 1
(CONTINUED) PROPERTIES OF THE STELLAR CENTER OF A $15 M_{\odot}$ STAR

	Si-dep		Si-shell		core-contr		pre-SN	
	FFN	LMP	FFN	LMP	FFN	LMP	FFN	LMP
$\log(t_b - t)$	4.75	4.93	4.50	4.53	3.51	3.57	-0.27	-0.60
T	$3.59 \cdot 10^9$	$3.78 \cdot 10^9$	$4.00 \cdot 10^9$	$4.13 \cdot 10^9$	$3.12 \cdot 10^9$	$3.55 \cdot 10^9$	$6.18 \cdot 10^9$	$7.16 \cdot 10^9$
ρ	$4.21 \cdot 10^7$	$5.87 \cdot 10^7$	$1.74 \cdot 10^8$	$3.20 \cdot 10^8$	$4.79 \cdot 10^8$	$5.41 \cdot 10^8$	$7.23 \cdot 10^9$	$9.08 \cdot 10^9$
Y_e	$4.63 \cdot 10^{-1}$	$4.67 \cdot 10^{-1}$	$4.52 \cdot 10^{-1}$	$4.49 \cdot 10^{-1}$	$4.42 \cdot 10^{-1}$	$4.45 \cdot 10^{-1}$	$4.30 \cdot 10^{-1}$	$4.32 \cdot 10^{-1}$
ϵ_{nuc}	$3.49 \cdot 10^{12}$	$2.65 \cdot 10^{12}$	$-5.27 \cdot 10^{10}$	$-1.11 \cdot 10^{11}$	$1.91 \cdot 10^{11}$	$-1.16 \cdot 10^{10}$	$-1.44 \cdot 10^{16}$	$-2.16 \cdot 10^{16}$
$\epsilon_{\nu, \text{weak}}$	$1.30 \cdot 10^{12}$	$1.73 \cdot 10^{12}$	$4.94 \cdot 10^{12}$	$1.91 \cdot 10^{12}$	$5.23 \cdot 10^{11}$	$6.06 \cdot 10^{11}$	$1.72 \cdot 10^{16}$	$2.46 \cdot 10^{16}$
$\epsilon_{\nu, \text{plas}}$	$5.20 \cdot 10^{12}$	$5.60 \cdot 10^{12}$	$1.82 \cdot 10^{12}$	$7.87 \cdot 10^{11}$	$7.64 \cdot 10^9$	$2.96 \cdot 10^{10}$	$3.00 \cdot 10^{11}$	$7.04 \cdot 10^{11}$
ϵ	$-3.00 \cdot 10^{12}$	$-4.68 \cdot 10^{12}$	$-6.81 \cdot 10^{12}$	$-2.80 \cdot 10^{12}$	$-3.39 \cdot 10^{11}$	$-6.47 \cdot 10^{11}$	$-3.16 \cdot 10^{16}$	$-4.61 \cdot 10^{16}$
S	1.50	1.41	1.07	$9.38 \cdot 10^{-1}$	$7.03 \cdot 10^{-1}$	$7.48 \cdot 10^{-1}$	$5.93 \cdot 10^{-1}$	$6.27 \cdot 10^{-1}$
S_e	$9.86 \cdot 10^{-1}$	$9.35 \cdot 10^{-1}$	$6.85 \cdot 10^{-1}$	$5.79 \cdot 10^{-1}$	$3.88 \cdot 10^{-1}$	$4.23 \cdot 10^{-1}$	$3.06 \cdot 10^{-1}$	$3.28 \cdot 10^{-1}$
S_{ion}	$3.79 \cdot 10^{-1}$	$3.65 \cdot 10^{-1}$	$3.42 \cdot 10^{-1}$	$3.32 \cdot 10^{-1}$	$3.07 \cdot 10^{-1}$	$3.15 \cdot 10^{-1}$	$2.83 \cdot 10^{-1}$	$2.94 \cdot 10^{-1}$
S_{rad}	$1.33 \cdot 10^{-1}$	$1.11 \cdot 10^{-1}$	$4.47 \cdot 10^{-2}$	$2.67 \cdot 10^{-2}$	$7.72 \cdot 10^{-3}$	$1.00 \cdot 10^{-2}$	$3.96 \cdot 10^{-3}$	$4.90 \cdot 10^{-3}$
S_{pair}	$2.86 \cdot 10^{-3}$	$1.92 \cdot 10^{-3}$	$1.69 \cdot 10^{-4}$	$3.35 \cdot 10^{-5}$	$1.93 \cdot 10^{-7}$	$6.93 \cdot 10^{-7}$	$1.20 \cdot 10^{-8}$	$3.86 \cdot 10^{-8}$
$Y(p)$	$6.80 \cdot 10^{-9}$	$1.42 \cdot 10^{-7}$	$2.93 \cdot 10^{-9}$	$1.97 \cdot 10^{-9}$	$1.54 \cdot 10^{-14}$	$3.37 \cdot 10^{-12}$	$4.02 \cdot 10^{-8}$	$7.28 \cdot 10^{-7}$
$\lambda_{p, \text{tot}}$	$3.08 \cdot 10^{-11}$	$1.26 \cdot 10^{-9}$	$1.79 \cdot 10^{-10}$	$3.76 \cdot 10^{-10}$	$5.16 \cdot 10^{-15}$	$1.54 \cdot 10^{-12}$	$2.40 \cdot 10^{-6}$	$6.72 \cdot 10^{-5}$
λ_{weak}	$7.33 \cdot 10^{-7}$	$9.14 \cdot 10^{-7}$	$4.21 \cdot 10^{-7}$	$2.43 \cdot 10^{-7}$	$-1.16 \cdot 10^{-7}$	$7.81 \cdot 10^{-9}$	$5.86 \cdot 10^{-3}$	$8.13 \cdot 10^{-3}$
$\lambda(\text{EC} + \beta^+)$	^{55}Fe $2.92 \cdot 10^{-7}$	^{55}Fe $3.35 \cdot 10^{-7}$	^{60}Co $5.81 \cdot 10^{-7}$	^{57}Fe $1.65 \cdot 10^{-7}$	^{60}Co $1.41 \cdot 10^{-7}$	^{57}Fe $6.80 \cdot 10^{-8}$	^{60}Co $1.66 \cdot 10^{-3}$	^{65}Ni $1.20 \cdot 10^{-3}$
	^{53}Mn $2.25 \cdot 10^{-7}$	^{54}Fe $1.54 \cdot 10^{-7}$	^{59}Co $2.70 \cdot 10^{-7}$	^{61}Ni $1.43 \cdot 10^{-7}$	^{59}Co $1.14 \cdot 10^{-8}$	^{55}Mn $3.10 \cdot 10^{-8}$	^{58}Mn $8.86 \cdot 10^{-4}$	^{59}Fe $6.14 \cdot 10^{-4}$
	^{57}Co $5.46 \cdot 10^{-8}$	^{57}Co $9.59 \cdot 10^{-8}$	^{54}Mn $2.51 \cdot 10^{-7}$	^{56}Fe $8.81 \cdot 10^{-8}$	^{57}Fe $7.16 \cdot 10^{-9}$	^{61}Ni $2.63 \cdot 10^{-8}$	^{59}Fe $8.27 \cdot 10^{-4}$	^{52}V $5.91 \cdot 10^{-4}$
	^{54}Fe $4.24 \cdot 10^{-8}$	^{59}Ni $8.75 \cdot 10^{-8}$	^{58}Co $1.81 \cdot 10^{-7}$	^{55}Mn $6.54 \cdot 10^{-8}$	^{55}Mn $4.32 \cdot 10^{-9}$	^{53}Cr $1.63 \cdot 10^{-8}$	^{52}V $7.50 \cdot 10^{-4}$	^{63}Ni $5.70 \cdot 10^{-4}$
	^{54}Mn $4.10 \cdot 10^{-8}$	^{53}Mn $5.98 \cdot 10^{-8}$	^{56}Fe $1.71 \cdot 10^{-7}$	^{53}Cr $4.47 \cdot 10^{-8}$	^{56}Mn $2.45 \cdot 10^{-9}$	^{56}Mn $1.21 \cdot 10^{-8}$	^{58}Fe $2.77 \cdot 10^{-4}$	^{62}Co $4.98 \cdot 10^{-4}$
$\lambda_{\text{EC, tot}}$	$7.52 \cdot 10^{-7}$	$9.09 \cdot 10^{-7}$	$1.94 \cdot 10^{-6}$	$7.10 \cdot 10^{-7}$	$1.69 \cdot 10^{-7}$	$2.04 \cdot 10^{-7}$	$5.87 \cdot 10^{-3}$	$8.14 \cdot 10^{-3}$
$\lambda_{\beta^+, \text{tot}}$	$9.49 \cdot 10^{-10}$	$6.10 \cdot 10^{-9}$	$8.12 \cdot 10^{-11}$	$5.44 \cdot 10^{-11}$	$3.86 \cdot 10^{-15}$	$4.88 \cdot 10^{-13}$	$7.99 \cdot 10^{-11}$	$5.03 \cdot 10^{-9}$
$\lambda(\text{PC} + \beta^-)$	^{55}Mn $1.22 \cdot 10^{-8}$	^{54}Mn $2.42 \cdot 10^{-10}$	^{59}Fe $5.98 \cdot 10^{-7}$	^{56}Mn $1.50 \cdot 10^{-7}$	^{60}Fe $8.19 \cdot 10^{-8}$	^{62}Co $4.50 \cdot 10^{-8}$	^{58}Mn $3.45 \cdot 10^{-6}$	^{64}Co $1.87 \cdot 10^{-6}$
	^{53}Cr $2.73 \cdot 10^{-9}$	^{58}Co $1.44 \cdot 10^{-10}$	^{60}Fe $1.97 \cdot 10^{-7}$	^{52}V $5.23 \cdot 10^{-8}$	^{57}Mn $6.24 \cdot 10^{-8}$	^{58}Mn $3.99 \cdot 10^{-8}$	^{54}V $1.23 \cdot 10^{-6}$	^{58}Mn $1.53 \cdot 10^{-6}$
	^{54}Cr $2.62 \cdot 10^{-9}$	^{56}Mn $1.26 \cdot 10^{-10}$	^{57}Mn $1.85 \cdot 10^{-7}$	^{57}Mn $4.76 \cdot 10^{-8}$	^{59}Fe $5.78 \cdot 10^{-8}$	^{56}Mn $2.18 \cdot 10^{-8}$	^{56}Cr $1.20 \cdot 10^{-6}$	^{54}V $1.05 \cdot 10^{-6}$
	^{57}Fe $1.10 \cdot 10^{-9}$	^{55}Mn $1.19 \cdot 10^{-10}$	^{54}Cr $1.74 \cdot 10^{-7}$	^{62}Co $4.14 \cdot 10^{-8}$	^{58}Mn $3.76 \cdot 10^{-8}$	^{55}Cr $1.84 \cdot 10^{-8}$	^{52}Ti $1.19 \cdot 10^{-6}$	^{52}Ti $7.31 \cdot 10^{-7}$
	^{56}Mn $8.99 \cdot 10^{-10}$	^{60}Co $7.48 \cdot 10^{-11}$	^{56}Mn $8.48 \cdot 10^{-8}$	^{55}Cr $4.05 \cdot 10^{-8}$	^{55}Cr $2.94 \cdot 10^{-8}$	^{57}Mn $1.81 \cdot 10^{-8}$	^{55}Cr $3.54 \cdot 10^{-7}$	^{56}Cr $5.57 \cdot 10^{-7}$
$\lambda_{\beta^-, \text{tot}}$	$2.05 \cdot 10^{-8}$	$8.59 \cdot 10^{-10}$	$1.52 \cdot 10^{-6}$	$4.67 \cdot 10^{-7}$	$2.86 \cdot 10^{-7}$	$1.96 \cdot 10^{-7}$	$7.93 \cdot 10^{-6}$	$8.08 \cdot 10^{-6}$

TABLE 2
 PROPERTIES OF THE STELLAR CENTER OF A 25 M_{\odot} STAR

	O-dep		O-shell		Si-ign		Si-burn	
	FFN	LMP	FFN	LMP	FFN	LMP	FFN	LMP
$\log(t_b - t)$	5.90	5.89	5.40	5.41	4.79	4.71	4.40	4.39
T	$2.49 \cdot 10^9$	$2.49 \cdot 10^9$	$2.36 \cdot 10^9$	$2.35 \cdot 10^9$	$3.21 \cdot 10^9$	$3.21 \cdot 10^9$	$3.62 \cdot 10^9$	$3.80 \cdot 10^9$
ρ	$5.73 \cdot 10^6$	$5.73 \cdot 10^6$	$2.61 \cdot 10^7$	$2.55 \cdot 10^7$	$6.88 \cdot 10^7$	$6.91 \cdot 10^7$	$2.17 \cdot 10^7$	$2.91 \cdot 10^7$
Y_e	$4.98 \cdot 10^{-1}$	$4.98 \cdot 10^{-1}$	$4.96 \cdot 10^{-1}$	$4.97 \cdot 10^{-1}$	$4.95 \cdot 10^{-1}$	$4.95 \cdot 10^{-1}$	$4.81 \cdot 10^{-1}$	$4.87 \cdot 10^{-1}$
ϵ_{nuc}	$1.79 \cdot 10^{12}$	$1.79 \cdot 10^{12}$	$7.60 \cdot 10^9$	$6.90 \cdot 10^9$	$1.42 \cdot 10^{13}$	$1.36 \cdot 10^{13}$	$1.04 \cdot 10^{14}$	$5.50 \cdot 10^{13}$
$\epsilon_{\nu, \text{weak}}$	$1.99 \cdot 10^9$	$2.04 \cdot 10^9$	$3.73 \cdot 10^9$	$3.39 \cdot 10^9$	$4.16 \cdot 10^{11}$	$1.88 \cdot 10^{11}$	$6.11 \cdot 10^{12}$	$8.06 \cdot 10^{12}$
$\epsilon_{\nu, \text{plas}}$	$1.34 \cdot 10^{12}$	$1.34 \cdot 10^{12}$	$8.02 \cdot 10^{10}$	$8.10 \cdot 10^{10}$	$6.63 \cdot 10^{11}$	$6.59 \cdot 10^{11}$	$1.34 \cdot 10^{13}$	$1.52 \cdot 10^{13}$
ϵ	$4.42 \cdot 10^{11}$	$4.42 \cdot 10^{11}$	$-7.63 \cdot 10^{10}$	$-7.75 \cdot 10^{10}$	$1.32 \cdot 10^{13}$	$1.28 \cdot 10^{13}$	$8.39 \cdot 10^{13}$	$3.17 \cdot 10^{13}$
S	2.40	2.40	1.54	1.54	1.48	1.48	1.99	1.91
S_e	1.42	1.42	$8.39 \cdot 10^{-1}$	$8.44 \cdot 10^{-1}$	$8.03 \cdot 10^{-1}$	$8.02 \cdot 10^{-1}$	1.25	1.20
S_{ion}	$6.44 \cdot 10^{-1}$	$6.44 \cdot 10^{-1}$	$6.38 \cdot 10^{-1}$	$6.39 \cdot 10^{-1}$	$6.18 \cdot 10^{-1}$	$6.18 \cdot 10^{-1}$	$4.64 \cdot 10^{-1}$	$4.76 \cdot 10^{-1}$
S_{rad}	$3.28 \cdot 10^{-1}$	$3.28 \cdot 10^{-1}$	$6.11 \cdot 10^{-2}$	$6.21 \cdot 10^{-2}$	$5.85 \cdot 10^{-2}$	$5.83 \cdot 10^{-2}$	$2.65 \cdot 10^{-1}$	$2.28 \cdot 10^{-1}$
S_{pair}	$1.14 \cdot 10^{-2}$	$1.14 \cdot 10^{-2}$	$1.64 \cdot 10^{-4}$	$1.71 \cdot 10^{-4}$	$2.48 \cdot 10^{-4}$	$2.45 \cdot 10^{-4}$	$1.38 \cdot 10^{-2}$	$1.03 \cdot 10^{-2}$
$Y(p)$	$1.84 \cdot 10^{-11}$	$1.84 \cdot 10^{-11}$	$1.36 \cdot 10^{-13}$	$1.34 \cdot 10^{-13}$	$8.14 \cdot 10^{-10}$	$8.99 \cdot 10^{-10}$	$2.58 \cdot 10^{-7}$	$4.01 \cdot 10^{-6}$
$\lambda_{p, \text{tot}}$	$1.40 \cdot 10^{-15}$	$1.40 \cdot 10^{-15}$	$9.21 \cdot 10^{-17}$	$8.63 \cdot 10^{-17}$	$7.41 \cdot 10^{-12}$	$8.28 \cdot 10^{-12}$	$4.74 \cdot 10^{-10}$	$1.32 \cdot 10^{-8}$
λ_{weak}	$1.43 \cdot 10^{-9}$	$1.41 \cdot 10^{-9}$	$3.14 \cdot 10^{-9}$	$2.84 \cdot 10^{-9}$	$2.55 \cdot 10^{-7}$	$1.14 \cdot 10^{-7}$	$3.53 \cdot 10^{-6}$	$3.45 \cdot 10^{-6}$
$\lambda(\text{EC} + \beta^+)$	^{37}Ar	^{37}Ar	^{35}Cl	^{35}Cl	^{55}Fe	^{35}Cl	^{54}Fe	^{53}Fe
	$3.30 \cdot 10^{-10}$	$3.41 \cdot 10^{-10}$	$1.19 \cdot 10^{-9}$	$1.13 \cdot 10^{-9}$	$5.52 \cdot 10^{-8}$	$2.19 \cdot 10^{-8}$	$9.86 \cdot 10^{-7}$	$7.43 \cdot 10^{-7}$
	^{32}S	^{36}Ar	^{37}Ar	^{37}Ar	^{53}Mn	^{33}S	^{55}Co	^{55}Co
	$2.76 \cdot 10^{-10}$	$2.92 \cdot 10^{-10}$	$6.06 \cdot 10^{-10}$	$5.73 \cdot 10^{-10}$	$4.50 \cdot 10^{-8}$	$2.18 \cdot 10^{-8}$	$9.84 \cdot 10^{-7}$	$6.46 \cdot 10^{-7}$
	^{35}Cl	^{35}Cl	^{33}S	^{33}S	^{54}Fe	^{32}S	^{55}Fe	^{56}Ni
	$2.70 \cdot 10^{-10}$	$2.71 \cdot 10^{-10}$	$5.73 \cdot 10^{-10}$	$5.19 \cdot 10^{-10}$	$3.20 \cdot 10^{-8}$	$1.92 \cdot 10^{-8}$	$4.88 \cdot 10^{-7}$	$6.10 \cdot 10^{-7}$
	^{36}Ar	^{32}S	^{32}S	^{32}S	^{33}S	^{55}Fe	^{56}Co	^{54}Fe
	$2.33 \cdot 10^{-10}$	$2.54 \cdot 10^{-10}$	$3.86 \cdot 10^{-10}$	$3.33 \cdot 10^{-10}$	$2.49 \cdot 10^{-8}$	$1.07 \cdot 10^{-8}$	$3.25 \cdot 10^{-7}$	$4.21 \cdot 10^{-7}$
	^{45}Ti	^{45}Ti	^{36}Ar	^{36}Ar	^{35}Cl	^{37}Ar	^{53}Mn	^{57}Ni
	$1.12 \cdot 10^{-10}$	$1.12 \cdot 10^{-10}$	$2.08 \cdot 10^{-10}$	$2.02 \cdot 10^{-10}$	$2.22 \cdot 10^{-8}$	$7.36 \cdot 10^{-9}$	$3.19 \cdot 10^{-7}$	$2.22 \cdot 10^{-7}$
$\lambda_{\text{EC, tot}}$	$1.40 \cdot 10^{-9}$	$1.38 \cdot 10^{-9}$	$3.13 \cdot 10^{-9}$	$2.83 \cdot 10^{-9}$	$2.54 \cdot 10^{-7}$	$1.13 \cdot 10^{-7}$	$3.49 \cdot 10^{-6}$	$3.30 \cdot 10^{-6}$
$\lambda_{\beta^+, \text{tot}}$	$3.04 \cdot 10^{-11}$	$2.72 \cdot 10^{-11}$	$7.92 \cdot 10^{-12}$	$6.92 \cdot 10^{-12}$	$1.08 \cdot 10^{-9}$	$9.40 \cdot 10^{-10}$	$3.72 \cdot 10^{-8}$	$1.53 \cdot 10^{-7}$
$\lambda(\text{PC} + \beta^-)$	^{32}P	^{32}P	^{32}P	^{32}P	^{32}P	^{32}P	^{55}Mn	^{54}Mn
	$3.48 \cdot 10^{-14}$	$1.86 \cdot 10^{-14}$	$6.07 \cdot 10^{-14}$	$3.13 \cdot 10^{-14}$	$3.03 \cdot 10^{-11}$	$1.41 \cdot 10^{-11}$	$2.86 \cdot 10^{-10}$	$8.01 \cdot 10^{-12}$
	^{36}Cl	^{36}Cl	^{36}Cl	^{36}Cl	^{55}Mn	^{54}Mn	^{53}Cr	^{55}Fe
	$6.77 \cdot 10^{-15}$	$5.98 \cdot 10^{-15}$	$3.47 \cdot 10^{-15}$	$3.01 \cdot 10^{-15}$	$1.32 \cdot 10^{-11}$	$1.82 \cdot 10^{-12}$	$4.39 \cdot 10^{-11}$	$2.75 \cdot 10^{-12}$
	^{46}Sc	^{46}Sc	^{46}Sc	^{54}Mn	^{53}Cr	^{36}Cl	^{54}Mn	^{58}Co
	$2.60 \cdot 10^{-15}$	$3.81 \cdot 10^{-16}$	$1.05 \cdot 10^{-15}$	$1.40 \cdot 10^{-16}$	$2.66 \cdot 10^{-12}$	$3.98 \cdot 10^{-13}$	$3.29 \cdot 10^{-11}$	$1.50 \cdot 10^{-12}$
	^{55}Mn	^{39}Ar	^{55}Mn	^{46}Sc	^{57}Fe	^{55}Mn	^{57}Fe	^{56}Co
	$1.63 \cdot 10^{-16}$	$1.54 \cdot 10^{-16}$	$3.95 \cdot 10^{-16}$	$1.31 \cdot 10^{-16}$	$9.47 \cdot 10^{-13}$	$3.13 \cdot 10^{-13}$	$2.90 \cdot 10^{-11}$	$1.26 \cdot 10^{-12}$
	^{33}P	^{54}Mn	^{33}P	^{39}Ar	^{54}Mn	^{28}Al	^{32}P	^{32}P
	$1.55 \cdot 10^{-16}$	$1.28 \cdot 10^{-16}$	$3.30 \cdot 10^{-16}$	$9.92 \cdot 10^{-17}$	$6.09 \cdot 10^{-13}$	$2.34 \cdot 10^{-13}$	$1.17 \cdot 10^{-11}$	$7.30 \cdot 10^{-13}$
$\lambda_{\beta^-, \text{tot}}$	$4.49 \cdot 10^{-14}$	$2.54 \cdot 10^{-14}$	$6.62 \cdot 10^{-14}$	$3.48 \cdot 10^{-14}$	$4.95 \cdot 10^{-11}$	$1.77 \cdot 10^{-11}$	$4.34 \cdot 10^{-10}$	$1.62 \cdot 10^{-11}$

(CONTINUED ON NEXT PAGE)

TABLE 2
(CONTINUED) PROPERTIES OF THE STELLAR CENTER OF A $25 M_{\odot}$ STAR

	Si-dep		Si-shell		core-contr		pre-SN	
	FFN	LMP	FFN	LMP	FFN	LMP	FFN	LMP
$\log(t_b - t)$	4.05	4.09	3.67	3.67	3.27	3.25	-0.31	-0.28
T	$3.89 \cdot 10^9$	$4.05 \cdot 10^9$	$4.81 \cdot 10^9$	$5.03 \cdot 10^9$	$4.44 \cdot 10^9$	$4.90 \cdot 10^9$	$7.13 \cdot 10^9$	$7.67 \cdot 10^9$
ρ	$2.52 \cdot 10^7$	$3.18 \cdot 10^7$	$1.37 \cdot 10^8$	$1.83 \cdot 10^8$	$2.26 \cdot 10^8$	$2.50 \cdot 10^8$	$2.65 \cdot 10^9$	$2.29 \cdot 10^9$
Y_e	$4.71 \cdot 10^{-1}$	$4.80 \cdot 10^{-1}$	$4.54 \cdot 10^{-1}$	$4.56 \cdot 10^{-1}$	$4.50 \cdot 10^{-1}$	$4.52 \cdot 10^{-1}$	$4.38 \cdot 10^{-1}$	$4.45 \cdot 10^{-1}$
ϵ_{nuc}	$3.10 \cdot 10^{13}$	$3.09 \cdot 10^{13}$	$-5.24 \cdot 10^{11}$	$-3.71 \cdot 10^{11}$	$-3.13 \cdot 10^{11}$	$-3.40 \cdot 10^{11}$	$-8.71 \cdot 10^{15}$	$-1.49 \cdot 10^{15}$
$\epsilon_{\nu, \text{weak}}$	$1.22 \cdot 10^{13}$	$1.24 \cdot 10^{13}$	$2.70 \cdot 10^{13}$	$1.00 \cdot 10^{13}$	$1.78 \cdot 10^{13}$	$8.54 \cdot 10^{12}$	$1.15 \cdot 10^{16}$	$5.54 \cdot 10^{15}$
$\epsilon_{\nu, \text{plas}}$	$2.36 \cdot 10^{13}$	$2.66 \cdot 10^{13}$	$2.15 \cdot 10^{13}$	$2.23 \cdot 10^{13}$	$3.76 \cdot 10^{12}$	$1.00 \cdot 10^{13}$	$6.99 \cdot 10^{12}$	$2.49 \cdot 10^{13}$
ϵ	$-4.79 \cdot 10^{12}$	$-8.14 \cdot 10^{12}$	$-4.90 \cdot 10^{13}$	$-3.27 \cdot 10^{13}$	$-2.19 \cdot 10^{13}$	$-1.89 \cdot 10^{13}$	$-2.03 \cdot 10^{16}$	$-7.05 \cdot 10^{15}$
S	1.94	1.88	1.33	1.27	1.08	1.14	$8.36 \cdot 10^{-1}$	$9.59 \cdot 10^{-1}$
S_e	1.25	1.22	$8.72 \cdot 10^{-1}$	$8.34 \cdot 10^{-1}$	$6.90 \cdot 10^{-1}$	$7.36 \cdot 10^{-1}$	$4.86 \cdot 10^{-1}$	$5.51 \cdot 10^{-1}$
S_{ion}	$3.88 \cdot 10^{-1}$	$3.88 \cdot 10^{-1}$	$3.56 \cdot 10^{-1}$	$3.55 \cdot 10^{-1}$	$3.42 \cdot 10^{-1}$	$3.45 \cdot 10^{-1}$	$3.34 \cdot 10^{-1}$	$3.84 \cdot 10^{-1}$
S_{rad}	$2.84 \cdot 10^{-1}$	$2.54 \cdot 10^{-1}$	$9.83 \cdot 10^{-2}$	$8.45 \cdot 10^{-2}$	$4.67 \cdot 10^{-2}$	$5.73 \cdot 10^{-2}$	$1.66 \cdot 10^{-2}$	$2.39 \cdot 10^{-2}$
S_{pair}	$1.79 \cdot 10^{-2}$	$1.43 \cdot 10^{-2}$	$1.78 \cdot 10^{-3}$	$1.22 \cdot 10^{-3}$	$2.13 \cdot 10^{-4}$	$4.12 \cdot 10^{-4}$	$8.57 \cdot 10^{-6}$	$3.19 \cdot 10^{-5}$
$Y(p)$	$1.02 \cdot 10^{-6}$	$1.11 \cdot 10^{-5}$	$5.37 \cdot 10^{-7}$	$1.68 \cdot 10^{-6}$	$2.05 \cdot 10^{-8}$	$3.27 \cdot 10^{-7}$	$5.05 \cdot 10^{-6}$	$5.50 \cdot 10^{-5}$
$\lambda_{p, \text{tot}}$	$2.84 \cdot 10^{-9}$	$4.93 \cdot 10^{-8}$	$2.94 \cdot 10^{-8}$	$1.59 \cdot 10^{-7}$	$2.27 \cdot 10^{-9}$	$4.95 \cdot 10^{-8}$	$5.68 \cdot 10^{-5}$	$5.15 \cdot 10^{-4}$
λ_{weak}	$6.61 \cdot 10^{-6}$	$5.43 \cdot 10^{-6}$	$2.84 \cdot 10^{-6}$	$2.84 \cdot 10^{-6}$	$7.95 \cdot 10^{-7}$	$1.26 \cdot 10^{-6}$	$3.48 \cdot 10^{-3}$	$1.58 \cdot 10^{-3}$
$\lambda(\text{EC} + \beta^+)$	^{55}Fe $1.43 \cdot 10^{-6}$	^{55}Co $1.02 \cdot 10^{-6}$	^{60}Co $1.85 \cdot 10^{-6}$	^{56}Fe $6.68 \cdot 10^{-7}$	^{60}Co $2.84 \cdot 10^{-6}$	^{56}Fe $4.52 \cdot 10^{-7}$	^{60}Co $2.28 \cdot 10^{-3}$	^1H $5.15 \cdot 10^{-4}$
	^{54}Fe $1.37 \cdot 10^{-6}$	^{54}Fe $9.35 \cdot 10^{-7}$	^{54}Mn $1.66 \cdot 10^{-6}$	^{55}Fe $5.03 \cdot 10^{-7}$	^{59}Co $8.83 \cdot 10^{-7}$	^{57}Fe $4.27 \cdot 10^{-7}$	^{57}Fe $3.00 \cdot 10^{-4}$	^{53}Cr $1.44 \cdot 10^{-4}$
	^{55}Co $1.27 \cdot 10^{-6}$	^{53}Fe $8.93 \cdot 10^{-7}$	^{55}Fe $1.25 \cdot 10^{-6}$	^{61}Ni $3.68 \cdot 10^{-7}$	^{54}Mn $6.99 \cdot 10^{-7}$	^{61}Ni $3.84 \cdot 10^{-7}$	^{59}Co $2.32 \cdot 10^{-4}$	^{57}Fe $1.13 \cdot 10^{-4}$
	^{56}Co $8.43 \cdot 10^{-7}$	^{56}Ni $6.77 \cdot 10^{-7}$	^{58}Co $9.95 \cdot 10^{-7}$	^{54}Mn $3.49 \cdot 10^{-7}$	^{57}Fe $4.16 \cdot 10^{-7}$	^{54}Mn $2.28 \cdot 10^{-7}$	^{52}V $1.88 \cdot 10^{-4}$	^{55}Mn $9.11 \cdot 10^{-5}$
	^{53}Mn $6.27 \cdot 10^{-7}$	^{57}Ni $5.05 \cdot 10^{-7}$	^{59}Co $9.88 \cdot 10^{-7}$	^{57}Fe $3.25 \cdot 10^{-7}$	^{56}Fe $3.52 \cdot 10^{-7}$	^{55}Mn $1.92 \cdot 10^{-7}$	^{54}Mn $1.28 \cdot 10^{-4}$	^{56}Fe $8.23 \cdot 10^{-5}$
$\lambda_{\text{EC, tot}}$	$6.56 \cdot 10^{-6}$	$5.20 \cdot 10^{-6}$	$9.54 \cdot 10^{-6}$	$3.85 \cdot 10^{-6}$	$6.39 \cdot 10^{-6}$	$2.84 \cdot 10^{-6}$	$3.76 \cdot 10^{-3}$	$1.63 \cdot 10^{-3}$
$\lambda_{\beta^+, \text{tot}}$	$5.78 \cdot 10^{-8}$	$2.34 \cdot 10^{-7}$	$1.21 \cdot 10^{-9}$	$5.74 \cdot 10^{-9}$	$1.23 \cdot 10^{-10}$	$1.52 \cdot 10^{-9}$	$1.04 \cdot 10^{-8}$	$1.44 \cdot 10^{-7}$
$\lambda(\text{PC} + \beta^-)$	^{55}Mn $3.20 \cdot 10^{-9}$	^{54}Mn $8.16 \cdot 10^{-11}$	^{59}Fe $1.85 \cdot 10^{-6}$	^{56}Mn $4.52 \cdot 10^{-7}$	^{59}Fe $1.97 \cdot 10^{-6}$	^{56}Mn $5.83 \cdot 10^{-7}$	^{58}Mn $6.60 \cdot 10^{-5}$	^{58}Mn $9.19 \cdot 10^{-6}$
	^{57}Fe $5.49 \cdot 10^{-10}$	^{58}Co $3.17 \cdot 10^{-11}$	^{57}Mn $1.10 \cdot 10^{-6}$	^{52}V $1.29 \cdot 10^{-7}$	^{57}Mn $1.03 \cdot 10^{-6}$	^{52}V $2.02 \cdot 10^{-7}$	^{56}Cr $6.33 \cdot 10^{-5}$	^{55}Cr $6.56 \cdot 10^{-6}$
	^{53}Cr $4.55 \cdot 10^{-10}$	^{55}Fe $2.52 \cdot 10^{-11}$	^{54}Cr $1.03 \cdot 10^{-6}$	^{60}Co $9.57 \cdot 10^{-8}$	^{60}Fe $9.00 \cdot 10^{-7}$	^{57}Mn $1.29 \cdot 10^{-7}$	^{52}Ti $5.48 \cdot 10^{-5}$	^{57}Mn $3.72 \cdot 10^{-6}$
	^{54}Mn $2.08 \cdot 10^{-10}$	^{57}Co $8.73 \cdot 10^{-12}$	^{60}Fe $5.77 \cdot 10^{-7}$	^{57}Mn $5.48 \cdot 10^{-8}$	^{54}Cr $5.18 \cdot 10^{-7}$	^{55}Cr $1.14 \cdot 10^{-7}$	^{55}Cr $4.45 \cdot 10^{-5}$	^{56}Cr $3.04 \cdot 10^{-6}$
	^{58}Co $1.35 \cdot 10^{-10}$	^{56}Co $6.96 \cdot 10^{-12}$	^{55}Mn $3.98 \cdot 10^{-7}$	^{55}Cr $4.29 \cdot 10^{-8}$	^{55}Cr $2.67 \cdot 10^{-7}$	^{60}Co $9.70 \cdot 10^{-8}$	^{57}Mn $1.54 \cdot 10^{-5}$	^{53}V $2.94 \cdot 10^{-6}$
$\lambda_{\beta^-, \text{tot}}$	$4.84 \cdot 10^{-9}$	$1.73 \cdot 10^{-10}$	$6.71 \cdot 10^{-6}$	$1.01 \cdot 10^{-6}$	$5.59 \cdot 10^{-6}$	$1.59 \cdot 10^{-6}$	$2.76 \cdot 10^{-4}$	$5.11 \cdot 10^{-5}$

TABLE 3
 PROPERTIES OF THE STELLAR CENTER OF A $40 M_{\odot}$ STAR

	O-dep		O-shell		Si-ign		Si-burn	
	FFN	LMP	FFN	LMP	FFN	LMP	FFN	LMP
$\log(t_b - t)$	5.41	5.41	5.20	5.20	4.92	4.84	4.51	4.53
T	$2.65 \cdot 10^9$	$2.65 \cdot 10^9$	$2.86 \cdot 10^9$	$2.85 \cdot 10^9$	$3.10 \cdot 10^9$	$3.13 \cdot 10^9$	$3.61 \cdot 10^9$	$3.70 \cdot 10^9$
ρ	$3.65 \cdot 10^6$	$3.65 \cdot 10^6$	$2.12 \cdot 10^7$	$2.06 \cdot 10^7$	$4.17 \cdot 10^7$	$4.59 \cdot 10^7$	$2.42 \cdot 10^7$	$3.61 \cdot 10^7$
Y_e	$4.98 \cdot 10^{-1}$	$4.98 \cdot 10^{-1}$	$4.96 \cdot 10^{-1}$	$4.97 \cdot 10^{-1}$	$4.94 \cdot 10^{-1}$	$4.96 \cdot 10^{-1}$	$4.87 \cdot 10^{-1}$	$4.93 \cdot 10^{-1}$
ϵ_{nuc}	$3.78 \cdot 10^{12}$	$3.81 \cdot 10^{12}$	$6.96 \cdot 10^{10}$	$3.19 \cdot 10^{10}$	$2.09 \cdot 10^{12}$	$2.01 \cdot 10^{12}$	$9.42 \cdot 10^{13}$	$5.84 \cdot 10^{13}$
$\epsilon_{\nu, \text{weak}}$	$1.94 \cdot 10^9$	$1.93 \cdot 10^9$	$3.72 \cdot 10^{10}$	$1.31 \cdot 10^{10}$	$1.56 \cdot 10^{11}$	$1.03 \cdot 10^{11}$	$5.77 \cdot 10^{12}$	$5.64 \cdot 10^{12}$
$\epsilon_{\nu, \text{plas}}$	$4.29 \cdot 10^{12}$	$4.29 \cdot 10^{12}$	$1.11 \cdot 10^{12}$	$1.12 \cdot 10^{12}$	$9.99 \cdot 10^{11}$	$9.75 \cdot 10^{11}$	$1.13 \cdot 10^{13}$	$8.69 \cdot 10^{12}$
ϵ	$-5.10 \cdot 10^{11}$	$-4.78 \cdot 10^{11}$	$-1.07 \cdot 10^{12}$	$-1.10 \cdot 10^{12}$	$9.31 \cdot 10^{11}$	$9.31 \cdot 10^{11}$	$7.71 \cdot 10^{13}$	$4.41 \cdot 10^{13}$
S	3.03	3.03	1.85	1.86	1.63	1.60	1.99	1.85
S_e	1.69	1.69	1.06	1.07	$9.12 \cdot 10^{-1}$	$8.95 \cdot 10^{-1}$	1.21	1.11
S_{ion}	$6.74 \cdot 10^{-1}$	$6.74 \cdot 10^{-1}$	$6.56 \cdot 10^{-1}$	$6.57 \cdot 10^{-1}$	$6.29 \cdot 10^{-1}$	$6.25 \cdot 10^{-1}$	$5.26 \cdot 10^{-1}$	$5.62 \cdot 10^{-1}$
S_{rad}	$6.17 \cdot 10^{-1}$	$6.17 \cdot 10^{-1}$	$1.33 \cdot 10^{-1}$	$1.37 \cdot 10^{-1}$	$8.65 \cdot 10^{-2}$	$8.13 \cdot 10^{-2}$	$2.35 \cdot 10^{-1}$	$1.70 \cdot 10^{-1}$
S_{pair}	$4.83 \cdot 10^{-2}$	$4.83 \cdot 10^{-2}$	$1.89 \cdot 10^{-3}$	$1.99 \cdot 10^{-3}$	$7.06 \cdot 10^{-4}$	$6.03 \cdot 10^{-4}$	$1.04 \cdot 10^{-2}$	$4.92 \cdot 10^{-3}$
$Y(p)$	$1.96 \cdot 10^{-10}$	$1.97 \cdot 10^{-10}$	$9.42 \cdot 10^{-11}$	$1.72 \cdot 10^{-10}$	$3.11 \cdot 10^{-10}$	$9.92 \cdot 10^{-10}$	$2.63 \cdot 10^{-7}$	$2.13 \cdot 10^{-6}$
$\lambda_{p, \text{tot}}$	$1.14 \cdot 10^{-14}$	$1.14 \cdot 10^{-14}$	$8.18 \cdot 10^{-14}$	$1.41 \cdot 10^{-13}$	$1.05 \cdot 10^{-12}$	$4.11 \cdot 10^{-12}$	$5.68 \cdot 10^{-10}$	$9.07 \cdot 10^{-9}$
λ_{weak}	$1.37 \cdot 10^{-9}$	$1.32 \cdot 10^{-9}$	$2.49 \cdot 10^{-8}$	$8.88 \cdot 10^{-9}$	$9.83 \cdot 10^{-8}$	$6.42 \cdot 10^{-8}$	$3.36 \cdot 10^{-6}$	$2.46 \cdot 10^{-6}$
$\lambda(\text{EC} + \beta^+)$	^{32}S	^{37}Ar	^{54}Fe	^{55}Fe	^{53}Mn	^{55}Fe	^{55}Co	^{56}Ni
	$2.88 \cdot 10^{-10}$	$2.83 \cdot 10^{-10}$	$6.38 \cdot 10^{-9}$	$1.72 \cdot 10^{-9}$	$2.81 \cdot 10^{-8}$	$1.27 \cdot 10^{-8}$	$1.15 \cdot 10^{-6}$	$5.32 \cdot 10^{-7}$
	^{37}Ar	^{32}S	^{53}Mn	^{32}S	^{55}Fe	^{54}Fe	^{54}Fe	^{53}Fe
	$2.74 \cdot 10^{-10}$	$2.64 \cdot 10^{-10}$	$5.63 \cdot 10^{-9}$	$1.37 \cdot 10^{-9}$	$2.39 \cdot 10^{-8}$	$1.17 \cdot 10^{-8}$	$9.18 \cdot 10^{-7}$	$4.90 \cdot 10^{-7}$
	^{35}Cl	^{36}Ar	^{55}Fe	^{54}Fe	^{54}Fe	^{32}S	^{55}Fe	^{55}Co
	$2.41 \cdot 10^{-10}$	$2.63 \cdot 10^{-10}$	$4.98 \cdot 10^{-9}$	$1.17 \cdot 10^{-9}$	$1.48 \cdot 10^{-8}$	$6.62 \cdot 10^{-9}$	$3.59 \cdot 10^{-7}$	$4.42 \cdot 10^{-7}$
	^{36}Ar	^{35}Cl	^{32}S	^{35}Cl	^{33}S	^{53}Mn	^{56}Co	^{54}Fe
	$2.18 \cdot 10^{-10}$	$2.40 \cdot 10^{-10}$	$1.23 \cdot 10^{-9}$	$9.55 \cdot 10^{-10}$	$6.06 \cdot 10^{-9}$	$6.22 \cdot 10^{-9}$	$2.92 \cdot 10^{-7}$	$2.51 \cdot 10^{-7}$
	^{33}S	^{33}S	^{33}S	^{33}S	^{35}Cl	^{33}S	^{53}Mn	^{52}Fe
	$1.06 \cdot 10^{-10}$	$9.51 \cdot 10^{-11}$	$1.17 \cdot 10^{-9}$	$8.23 \cdot 10^{-10}$	$4.23 \cdot 10^{-9}$	$4.73 \cdot 10^{-9}$	$2.44 \cdot 10^{-7}$	$1.48 \cdot 10^{-7}$
$\lambda_{\text{EC, tot}}$	$1.29 \cdot 10^{-9}$	$1.25 \cdot 10^{-9}$	$2.46 \cdot 10^{-8}$	$8.68 \cdot 10^{-9}$	$9.78 \cdot 10^{-8}$	$6.34 \cdot 10^{-8}$	$3.33 \cdot 10^{-6}$	$2.37 \cdot 10^{-6}$
$\lambda_{\beta^+, \text{tot}}$	$7.91 \cdot 10^{-11}$	$7.04 \cdot 10^{-11}$	$2.16 \cdot 10^{-10}$	$2.07 \cdot 10^{-10}$	$5.30 \cdot 10^{-10}$	$7.85 \cdot 10^{-10}$	$3.41 \cdot 10^{-8}$	$8.61 \cdot 10^{-8}$
$\lambda(\text{PC} + \beta^-)$	^{32}P	^{32}P	^{32}P	^{32}P	^{32}P	^{32}P	^{55}Mn	^{54}Mn
	$1.78 \cdot 10^{-13}$	$9.10 \cdot 10^{-14}$	$2.55 \cdot 10^{-12}$	$5.22 \cdot 10^{-13}$	$1.98 \cdot 10^{-11}$	$3.32 \cdot 10^{-12}$	$1.10 \cdot 10^{-10}$	$1.63 \cdot 10^{-12}$
	^{36}Cl	^{36}Cl	^{55}Mn	^{54}Mn	^{55}Mn	^{54}Mn	^{53}Cr	^{55}Fe
	$2.30 \cdot 10^{-14}$	$2.16 \cdot 10^{-14}$	$1.72 \cdot 10^{-12}$	$2.33 \cdot 10^{-13}$	$1.87 \cdot 10^{-11}$	$2.24 \cdot 10^{-12}$	$1.81 \cdot 10^{-11}$	$5.77 \cdot 10^{-13}$
	^{46}Sc	^{46}Sc	^{53}Cr	^{36}Cl	^{53}Cr	^{55}Mn	^{54}Mn	^{32}P
	$7.10 \cdot 10^{-15}$	$1.05 \cdot 10^{-15}$	$2.20 \cdot 10^{-13}$	$2.35 \cdot 10^{-14}$	$3.88 \cdot 10^{-12}$	$2.19 \cdot 10^{-13}$	$1.63 \cdot 10^{-11}$	$5.49 \cdot 10^{-13}$
	^{55}Mn	^{39}Ar	^{54}Mn	^{55}Mn	^{57}Fe	^{50}V	^{32}P	^{56}Co
	$9.57 \cdot 10^{-16}$	$6.59 \cdot 10^{-16}$	$1.36 \cdot 10^{-13}$	$1.79 \cdot 10^{-14}$	$8.36 \cdot 10^{-13}$	$1.55 \cdot 10^{-13}$	$1.25 \cdot 10^{-11}$	$3.14 \cdot 10^{-13}$
	^{33}P	^{54}Mn	^{57}Fe	^{50}V	^{54}Mn	^{53}Cr	^{57}Fe	^{58}Co
	$8.98 \cdot 10^{-16}$	$5.63 \cdot 10^{-16}$	$6.56 \cdot 10^{-14}$	$1.27 \cdot 10^{-14}$	$7.45 \cdot 10^{-13}$	$9.08 \cdot 10^{-14}$	$1.08 \cdot 10^{-11}$	$2.66 \cdot 10^{-13}$
$\lambda_{\beta^-, \text{tot}}$	$2.12 \cdot 10^{-13}$	$1.16 \cdot 10^{-13}$	$4.83 \cdot 10^{-12}$	$8.38 \cdot 10^{-13}$	$4.60 \cdot 10^{-11}$	$6.43 \cdot 10^{-12}$	$1.82 \cdot 10^{-10}$	$3.75 \cdot 10^{-12}$

(CONTINUED ON NEXT PAGE)

TABLE 3
(CONTINUED) PROPERTIES OF THE STELLAR CENTER OF A $40 M_{\odot}$ STAR

	Si-dep		Si-shell		core-contr		pre-SN	
	FFN	LMP	FFN	LMP	FFN	LMP	FFN	LMP
$\log(t_b - t)$	3.78	3.75	3.11	3.15	2.65	2.63	-0.33	-0.22
T	$3.98 \cdot 10^9$	$4.11 \cdot 10^9$	$5.17 \cdot 10^9$	$5.38 \cdot 10^9$	$5.17 \cdot 10^9$	$5.62 \cdot 10^9$	$7.68 \cdot 10^9$	$8.01 \cdot 10^9$
ρ	$2.47 \cdot 10^7$	$2.98 \cdot 10^7$	$1.35 \cdot 10^8$	$1.47 \cdot 10^8$	$2.47 \cdot 10^8$	$2.47 \cdot 10^8$	$2.50 \cdot 10^9$	$1.68 \cdot 10^9$
Y_e	$4.71 \cdot 10^{-1}$	$4.80 \cdot 10^{-1}$	$4.54 \cdot 10^{-1}$	$4.59 \cdot 10^{-1}$	$4.49 \cdot 10^{-1}$	$4.53 \cdot 10^{-1}$	$4.39 \cdot 10^{-1}$	$4.47 \cdot 10^{-1}$
ϵ_{nuc}	$2.50 \cdot 10^{13}$	$3.32 \cdot 10^{13}$	$-8.67 \cdot 10^{11}$	$2.16 \cdot 10^{12}$	$-1.35 \cdot 10^{12}$	$-6.10 \cdot 10^{11}$	$-1.10 \cdot 10^{16}$	$5.76 \cdot 10^{14}$
$\epsilon_{\nu, \text{weak}}$	$1.62 \cdot 10^{13}$	$1.46 \cdot 10^{13}$	$5.26 \cdot 10^{13}$	$2.00 \cdot 10^{13}$	$8.26 \cdot 10^{13}$	$3.09 \cdot 10^{13}$	$1.62 \cdot 10^{16}$	$6.71 \cdot 10^{15}$
$\epsilon_{\nu, \text{plas}}$	$3.05 \cdot 10^{13}$	$3.30 \cdot 10^{13}$	$4.72 \cdot 10^{13}$	$6.30 \cdot 10^{13}$	$1.88 \cdot 10^{13}$	$4.63 \cdot 10^{13}$	$2.12 \cdot 10^{13}$	$8.30 \cdot 10^{13}$
ϵ	$-2.17 \cdot 10^{13}$	$-1.44 \cdot 10^{13}$	$-1.01 \cdot 10^{14}$	$-8.08 \cdot 10^{13}$	$-1.03 \cdot 10^{14}$	$-7.79 \cdot 10^{13}$	$-2.72 \cdot 10^{16}$	$-6.22 \cdot 10^{15}$
S	2.00	1.95	1.43	1.46	1.19	1.29	$9.26 \cdot 10^{-1}$	1.15
S_e	1.28	1.26	$9.34 \cdot 10^{-1}$	$9.50 \cdot 10^{-1}$	$7.71 \cdot 10^{-1}$	$8.35 \cdot 10^{-1}$	$5.31 \cdot 10^{-1}$	$6.33 \cdot 10^{-1}$
S_{ion}	$3.84 \cdot 10^{-1}$	$3.89 \cdot 10^{-1}$	$3.64 \cdot 10^{-1}$	$3.72 \cdot 10^{-1}$	$3.49 \cdot 10^{-1}$	$3.62 \cdot 10^{-1}$	$3.72 \cdot 10^{-1}$	$4.77 \cdot 10^{-1}$
S_{rad}	$3.11 \cdot 10^{-1}$	$2.83 \cdot 10^{-1}$	$1.24 \cdot 10^{-1}$	$1.29 \cdot 10^{-1}$	$6.81 \cdot 10^{-2}$	$8.73 \cdot 10^{-2}$	$2.21 \cdot 10^{-2}$	$3.72 \cdot 10^{-2}$
S_{pair}	$2.23 \cdot 10^{-2}$	$1.83 \cdot 10^{-2}$	$3.40 \cdot 10^{-3}$	$3.73 \cdot 10^{-3}$	$7.04 \cdot 10^{-4}$	$1.44 \cdot 10^{-3}$	$2.48 \cdot 10^{-5}$	$1.39 \cdot 10^{-4}$
$Y(p)$	$2.66 \cdot 10^{-6}$	$1.84 \cdot 10^{-5}$	$2.86 \cdot 10^{-6}$	$1.47 \cdot 10^{-5}$	$6.06 \cdot 10^{-7}$	$6.90 \cdot 10^{-6}$	$2.09 \cdot 10^{-5}$	$1.77 \cdot 10^{-4}$
$\lambda_{p, \text{tot}}$	$7.71 \cdot 10^{-9}$	$7.76 \cdot 10^{-8}$	$1.75 \cdot 10^{-7}$	$1.12 \cdot 10^{-6}$	$9.52 \cdot 10^{-8}$	$1.24 \cdot 10^{-6}$	$2.21 \cdot 10^{-4}$	$1.03 \cdot 10^{-3}$
λ_{weak}	$8.64 \cdot 10^{-6}$	$6.29 \cdot 10^{-6}$	$6.36 \cdot 10^{-6}$	$6.84 \cdot 10^{-6}$	$2.21 \cdot 10^{-6}$	$4.69 \cdot 10^{-6}$	$4.37 \cdot 10^{-3}$	$1.76 \cdot 10^{-3}$
$\lambda(\text{EC} + \beta^+)$	^{55}Co $1.83 \cdot 10^{-6}$	^{55}Co $1.21 \cdot 10^{-6}$	^{54}Mn $3.37 \cdot 10^{-6}$	^{55}Fe $1.37 \cdot 10^{-6}$	^{60}Co $1.17 \cdot 10^{-5}$	^{56}Fe $1.27 \cdot 10^{-6}$	^{60}Co $2.73 \cdot 10^{-3}$	^1H $1.03 \cdot 10^{-3}$
	^{55}Fe $1.60 \cdot 10^{-6}$	^{53}Fe $1.04 \cdot 10^{-6}$	^{60}Co $3.25 \cdot 10^{-6}$	^1H $1.12 \cdot 10^{-6}$	^{59}Co $3.21 \cdot 10^{-6}$	^1H $1.24 \cdot 10^{-6}$	^{57}Fe $3.76 \cdot 10^{-4}$	^{53}Cr $9.73 \cdot 10^{-5}$
	^{56}Co $1.45 \cdot 10^{-6}$	^{54}Fe $9.44 \cdot 10^{-7}$	^{55}Fe $2.55 \cdot 10^{-6}$	^{56}Fe $1.05 \cdot 10^{-6}$	^{54}Mn $3.17 \cdot 10^{-6}$	^{57}Fe $9.44 \cdot 10^{-7}$	^{59}Co $3.02 \cdot 10^{-4}$	^{57}Fe $7.53 \cdot 10^{-5}$
	^{54}Fe $1.27 \cdot 10^{-6}$	^{56}Ni $9.15 \cdot 10^{-7}$	^{58}Co $1.79 \cdot 10^{-6}$	^{54}Mn $5.93 \cdot 10^{-7}$	^{57}Fe $1.69 \cdot 10^{-6}$	^{54}Mn $7.83 \cdot 10^{-7}$	^{52}V $2.61 \cdot 10^{-4}$	^{56}Fe $6.35 \cdot 10^{-5}$
	^{57}Co $8.86 \cdot 10^{-7}$	^{57}Ni $6.30 \cdot 10^{-7}$	^{59}Co $1.76 \cdot 10^{-6}$	^{53}Mn $4.90 \cdot 10^{-7}$	^{58}Co $1.17 \cdot 10^{-6}$	^{61}Ni $7.56 \cdot 10^{-7}$	^{54}Mn $2.24 \cdot 10^{-4}$	^{55}Mn $6.32 \cdot 10^{-5}$
$\lambda_{\text{EC, tot}}$	$8.57 \cdot 10^{-6}$	$5.99 \cdot 10^{-6}$	$1.82 \cdot 10^{-5}$	$7.86 \cdot 10^{-6}$	$2.54 \cdot 10^{-5}$	$9.31 \cdot 10^{-6}$	$4.90 \cdot 10^{-3}$	$1.84 \cdot 10^{-3}$
$\lambda_{\beta^+, \text{tot}}$	$8.55 \cdot 10^{-8}$	$3.00 \cdot 10^{-7}$	$2.90 \cdot 10^{-9}$	$2.98 \cdot 10^{-8}$	$5.41 \cdot 10^{-10}$	$1.22 \cdot 10^{-8}$	$4.57 \cdot 10^{-8}$	$3.03 \cdot 10^{-7}$
$\lambda(\text{PC} + \beta^-)$	^{55}Mn $3.43 \cdot 10^{-9}$	^{54}Mn $7.95 \cdot 10^{-11}$	^{59}Fe $2.82 \cdot 10^{-6}$	^{56}Mn $4.29 \cdot 10^{-7}$	^{57}Mn $6.49 \cdot 10^{-6}$	^{56}Mn $1.48 \cdot 10^{-6}$	^{56}Cr $1.26 \cdot 10^{-4}$	^{58}Mn $1.22 \cdot 10^{-5}$
	^{57}Fe $1.06 \cdot 10^{-9}$	^{58}Co $3.42 \cdot 10^{-11}$	^{57}Mn $2.26 \cdot 10^{-6}$	^{52}V $1.13 \cdot 10^{-7}$	^{59}Fe $5.88 \cdot 10^{-6}$	^{52}V $5.54 \cdot 10^{-7}$	^{58}Mn $1.17 \cdot 10^{-4}$	^{55}Cr $9.82 \cdot 10^{-6}$
	^{58}Co $3.99 \cdot 10^{-10}$	^{55}Fe $2.98 \cdot 10^{-11}$	^{54}Cr $1.87 \cdot 10^{-6}$	^{60}Co $1.09 \cdot 10^{-7}$	^{60}Fe $3.16 \cdot 10^{-6}$	^{57}Mn $3.33 \cdot 10^{-7}$	^{52}Ti $1.02 \cdot 10^{-4}$	^{57}Mn $5.91 \cdot 10^{-6}$
	^{53}Cr $3.07 \cdot 10^{-10}$	^{57}Co $1.09 \cdot 10^{-11}$	^{60}Fe $8.87 \cdot 10^{-7}$	^{55}Mn $7.39 \cdot 10^{-8}$	^{54}Cr $1.89 \cdot 10^{-6}$	^{55}Cr $3.23 \cdot 10^{-7}$	^{55}Cr $8.57 \cdot 10^{-5}$	^{56}Mn $5.34 \cdot 10^{-6}$
	^{54}Mn $1.99 \cdot 10^{-10}$	^{56}Co $9.52 \cdot 10^{-12}$	^{55}Mn $7.09 \cdot 10^{-7}$	^{53}Cr $4.04 \cdot 10^{-8}$	^{55}Cr $1.63 \cdot 10^{-6}$	^{60}Co $2.61 \cdot 10^{-7}$	^{57}Mn $2.96 \cdot 10^{-5}$	^{53}V $4.48 \cdot 10^{-6}$
$\lambda_{\beta^-, \text{tot}}$	$5.86 \cdot 10^{-9}$	$1.83 \cdot 10^{-10}$	$1.18 \cdot 10^{-5}$	$1.04 \cdot 10^{-6}$	$2.32 \cdot 10^{-5}$	$4.63 \cdot 10^{-6}$	$5.28 \cdot 10^{-4}$	$7.76 \cdot 10^{-5}$

TABLE 4
 \int RATE / TOTAL RATE dY_e – MOST IMPORTANT CONTRIBUTORS TO ΔY_e , LMP $15M_\odot$

ion	total	EC	β^-	β^+
^{57}Fe	$1.13 \cdot 10^{-2}$	$1.13 \cdot 10^{-2}$	$4.64 \cdot 10^{-5}$	$4.25 \cdot 10^{-8}$
^{55}Fe	$1.01 \cdot 10^{-2}$	$1.00 \cdot 10^{-2}$	$8.33 \cdot 10^{-8}$	$9.91 \cdot 10^{-6}$
^{61}Ni	$7.56 \cdot 10^{-3}$	$7.56 \cdot 10^{-3}$	$1.47 \cdot 10^{-7}$	$7.44 \cdot 10^{-8}$
^{54}Fe	$6.92 \cdot 10^{-3}$	$6.91 \cdot 10^{-3}$	$4.17 \cdot 10^{-13}$	$9.52 \cdot 10^{-6}$
^{56}Fe	$5.87 \cdot 10^{-3}$	$5.87 \cdot 10^{-3}$	$4.78 \cdot 10^{-7}$	$1.43 \cdot 10^{-7}$
^{55}Mn	$5.15 \cdot 10^{-3}$	$5.28 \cdot 10^{-3}$	$1.24 \cdot 10^{-4}$	$4.38 \cdot 10^{-8}$
^{53}Cr	$4.28 \cdot 10^{-3}$	$4.33 \cdot 10^{-3}$	$5.27 \cdot 10^{-5}$	$9.19 \cdot 10^{-9}$
^{35}Cl	$3.48 \cdot 10^{-3}$	$3.48 \cdot 10^{-3}$	$9.81 \cdot 10^{-15}$	$2.86 \cdot 10^{-8}$
^{53}Mn	$3.44 \cdot 10^{-3}$	$3.44 \cdot 10^{-3}$	$5.53 \cdot 10^{-9}$	$7.34 \cdot 10^{-6}$
^{33}S	$3.09 \cdot 10^{-3}$	$3.09 \cdot 10^{-3}$	$3.36 \cdot 10^{-14}$	$4.19 \cdot 10^{-9}$
^{56}Mn	$-4.05 \cdot 10^{-3}$	$2.23 \cdot 10^{-3}$	$6.28 \cdot 10^{-3}$	$2.89 \cdot 10^{-9}$
^{58}Mn	$-4.32 \cdot 10^{-3}$	$4.34 \cdot 10^{-5}$	$4.37 \cdot 10^{-3}$	$8.64 \cdot 10^{-12}$
^{62}Co	$-3.54 \cdot 10^{-3}$	$2.91 \cdot 10^{-4}$	$3.83 \cdot 10^{-3}$	$7.06 \cdot 10^{-11}$
^{57}Mn	$-2.34 \cdot 10^{-3}$	$2.36 \cdot 10^{-5}$	$2.36 \cdot 10^{-3}$	$2.47 \cdot 10^{-11}$
^{55}Cr	$-2.29 \cdot 10^{-3}$	$4.10 \cdot 10^{-5}$	$2.33 \cdot 10^{-3}$	$2.30 \cdot 10^{-11}$
^{52}V	$-5.33 \cdot 10^{-4}$	$1.61 \cdot 10^{-3}$	$2.14 \cdot 10^{-3}$	$7.96 \cdot 10^{-10}$
^{53}V	$-1.54 \cdot 10^{-3}$	$8.92 \cdot 10^{-5}$	$1.63 \cdot 10^{-3}$	$2.18 \cdot 10^{-11}$
^{63}Co	$-9.55 \cdot 10^{-4}$	$2.56 \cdot 10^{-5}$	$9.81 \cdot 10^{-4}$	$1.53 \cdot 10^{-12}$
^{60}Co	$8.18 \cdot 10^{-5}$	$1.06 \cdot 10^{-3}$	$9.76 \cdot 10^{-4}$	$5.45 \cdot 10^{-8}$
^{64}Co	$-7.20 \cdot 10^{-4}$...	$7.20 \cdot 10^{-4}$...

NOTE.— The first section list the ten ions most important for decreasing Y_e (electron capture and β^+ -decay), the second section those which dominate β^- -decay.

TABLE 5
 \int RATE / TOTAL RATE dY_e – MOST IMPORTANT CONTRIBUTORS TO ΔY_e , LMP $25M_\odot$

ion	total	EC	β^-	β^+
^{55}Fe	$6.27 \cdot 10^{-3}$	$6.25 \cdot 10^{-3}$	$5.36 \cdot 10^{-7}$	$1.93 \cdot 10^{-5}$
^{54}Fe	$5.00 \cdot 10^{-3}$	$4.97 \cdot 10^{-3}$	$2.54 \cdot 10^{-11}$	$2.53 \cdot 10^{-5}$
^{56}Fe	$4.45 \cdot 10^{-3}$	$4.45 \cdot 10^{-3}$	$2.22 \cdot 10^{-6}$	$6.32 \cdot 10^{-7}$
^{55}Co	$4.36 \cdot 10^{-3}$	$4.26 \cdot 10^{-3}$	$7.73 \cdot 10^{-15}$	$1.03 \cdot 10^{-4}$
^{53}Fe	$4.23 \cdot 10^{-3}$	$3.87 \cdot 10^{-3}$	$6.05 \cdot 10^{-16}$	$3.57 \cdot 10^{-4}$
^{56}Ni	$3.69 \cdot 10^{-3}$	$3.68 \cdot 10^{-3}$...	$1.27 \cdot 10^{-5}$
^{57}Fe	$3.44 \cdot 10^{-3}$	$3.52 \cdot 10^{-3}$	$8.11 \cdot 10^{-5}$	$1.89 \cdot 10^{-7}$
^{61}Ni	$2.90 \cdot 10^{-3}$	$2.90 \cdot 10^{-3}$	$6.16 \cdot 10^{-7}$	$2.73 \cdot 10^{-7}$
^{54}Mn	$2.28 \cdot 10^{-3}$	$2.30 \cdot 10^{-3}$	$2.95 \cdot 10^{-5}$	$8.45 \cdot 10^{-6}$
^{57}Ni	$1.90 \cdot 10^{-3}$	$1.86 \cdot 10^{-3}$	$3.13 \cdot 10^{-14}$	$4.26 \cdot 10^{-5}$
^{56}Mn	$-3.27 \cdot 10^{-3}$	$4.42 \cdot 10^{-4}$	$3.71 \cdot 10^{-3}$	$1.65 \cdot 10^{-8}$
^{52}V	$-1.01 \cdot 10^{-3}$	$2.69 \cdot 10^{-4}$	$1.28 \cdot 10^{-3}$	$7.34 \cdot 10^{-9}$
^{58}Mn	$-9.74 \cdot 10^{-4}$	$4.57 \cdot 10^{-7}$	$9.74 \cdot 10^{-4}$	$2.28 \cdot 10^{-11}$
^{55}Cr	$-9.38 \cdot 10^{-4}$	$1.42 \cdot 10^{-6}$	$9.39 \cdot 10^{-4}$	$1.91 \cdot 10^{-10}$
^{57}Mn	$-9.22 \cdot 10^{-4}$	$9.05 \cdot 10^{-7}$	$9.23 \cdot 10^{-4}$	$2.35 \cdot 10^{-10}$
^{62}Co	$-6.59 \cdot 10^{-4}$	$8.46 \cdot 10^{-6}$	$6.68 \cdot 10^{-4}$	$2.31 \cdot 10^{-10}$
^{60}Co	$-2.78 \cdot 10^{-4}$	$3.76 \cdot 10^{-4}$	$6.55 \cdot 10^{-4}$	$1.67 \cdot 10^{-7}$
^{53}V	$-6.05 \cdot 10^{-4}$	$2.65 \cdot 10^{-6}$	$6.08 \cdot 10^{-4}$	$1.32 \cdot 10^{-10}$
^{59}Fe	$-4.07 \cdot 10^{-4}$	$2.36 \cdot 10^{-5}$	$4.30 \cdot 10^{-4}$	$9.14 \cdot 10^{-10}$
^{61}Co	$-2.78 \cdot 10^{-4}$	$3.50 \cdot 10^{-5}$	$3.13 \cdot 10^{-4}$	$3.03 \cdot 10^{-9}$

TABLE 6
 \int RATE / TOTAL RATE dY_e – MOST IMPORTANT CONTRIBUTORS TO ΔY_e , LMP 40 M_\odot

ion	total	EC	β^-	β^+
^{55}Fe	$5.93 \cdot 10^{-3}$	$5.91 \cdot 10^{-3}$	$6.91 \cdot 10^{-7}$	$2.27 \cdot 10^{-5}$
^{54}Fe	$5.21 \cdot 10^{-3}$	$5.19 \cdot 10^{-3}$	$4.40 \cdot 10^{-11}$	$2.77 \cdot 10^{-5}$
^1H	$5.01 \cdot 10^{-3}$	$5.01 \cdot 10^{-3}$
^{55}Co	$4.38 \cdot 10^{-3}$	$4.27 \cdot 10^{-3}$	$1.35 \cdot 10^{-14}$	$1.15 \cdot 10^{-4}$
^{53}Fe	$4.28 \cdot 10^{-3}$	$3.90 \cdot 10^{-3}$	$1.03 \cdot 10^{-15}$	$3.79 \cdot 10^{-4}$
^{56}Ni	$3.74 \cdot 10^{-3}$	$3.72 \cdot 10^{-3}$...	$1.57 \cdot 10^{-5}$
^{56}Fe	$3.04 \cdot 10^{-3}$	$3.04 \cdot 10^{-3}$	$3.90 \cdot 10^{-6}$	$1.26 \cdot 10^{-6}$
^{57}Ni	$1.95 \cdot 10^{-3}$	$1.90 \cdot 10^{-3}$	$5.62 \cdot 10^{-14}$	$4.77 \cdot 10^{-5}$
^{54}Mn	$1.80 \cdot 10^{-3}$	$1.82 \cdot 10^{-3}$	$3.12 \cdot 10^{-5}$	$1.04 \cdot 10^{-5}$
^{53}Mn	$1.80 \cdot 10^{-3}$	$1.78 \cdot 10^{-3}$	$8.13 \cdot 10^{-8}$	$1.17 \cdot 10^{-5}$
^{56}Mn	$-1.93 \cdot 10^{-3}$	$2.10 \cdot 10^{-4}$	$2.14 \cdot 10^{-3}$	$3.21 \cdot 10^{-8}$
^{52}V	$-6.49 \cdot 10^{-4}$	$1.32 \cdot 10^{-4}$	$7.80 \cdot 10^{-4}$	$1.66 \cdot 10^{-8}$
^{55}Cr	$-5.32 \cdot 10^{-4}$	$8.86 \cdot 10^{-7}$	$5.33 \cdot 10^{-4}$	$5.00 \cdot 10^{-10}$
^{57}Mn	$-5.03 \cdot 10^{-4}$	$5.89 \cdot 10^{-7}$	$5.03 \cdot 10^{-4}$	$5.84 \cdot 10^{-10}$
^{58}Mn	$-4.70 \cdot 10^{-4}$	$2.39 \cdot 10^{-7}$	$4.70 \cdot 10^{-4}$	$4.78 \cdot 10^{-11}$
^{60}Co	$-2.01 \cdot 10^{-4}$	$2.06 \cdot 10^{-4}$	$4.07 \cdot 10^{-4}$	$2.39 \cdot 10^{-7}$
^{53}V	$-3.30 \cdot 10^{-4}$	$1.58 \cdot 10^{-6}$	$3.32 \cdot 10^{-4}$	$3.31 \cdot 10^{-10}$
^{59}Fe	$-2.93 \cdot 10^{-4}$	$1.11 \cdot 10^{-5}$	$3.05 \cdot 10^{-4}$	$2.09 \cdot 10^{-9}$
^{62}Co	$-2.96 \cdot 10^{-4}$	$3.42 \cdot 10^{-6}$	$2.99 \cdot 10^{-4}$	$3.89 \cdot 10^{-10}$
^{54}Cr	$-2.44 \cdot 10^{-4}$	$2.73 \cdot 10^{-5}$	$2.71 \cdot 10^{-4}$	$7.43 \cdot 10^{-9}$

TABLE 7
INTEGRATED VALUES, SUMMARY TABLE

model	F	F_{EC}	F_{β^+}	F_{β^-}	E_{weak} erg g ⁻¹	E_{plas} erg g ⁻¹	E_{EC} erg g ⁻¹	E_{β^-} erg g ⁻¹
FFN, 15M _⊙	3.39·10 ⁻¹	3.94·10 ⁻¹	7.04·10 ⁻⁴	5.49·10 ⁻²	7.09·10 ¹⁷	1.20·10 ¹⁸	6.34·10 ¹⁷	7.44·10 ¹⁶
LMP, 15M _⊙	2.60·10 ⁻¹	2.86·10 ⁻¹	1.98·10 ⁻³	2.88·10 ⁻²	5.39·10 ¹⁷	1.24·10 ¹⁸	4.88·10 ¹⁷	5.10·10 ¹⁶
FFN, 25M _⊙	2.30·10 ⁻¹	2.78·10 ⁻¹	1.84·10 ⁻³	4.96·10 ⁻²	5.60·10 ¹⁷	1.00·10 ¹⁸	4.82·10 ¹⁷	7.76·10 ¹⁶
LMP, 25M _⊙	1.63·10 ⁻¹	1.70·10 ⁻¹	5.49·10 ⁻³	1.19·10 ⁻²	4.16·10 ¹⁷	9.94·10 ¹⁷	3.92·10 ¹⁷	2.40·10 ¹⁶
FFN, 40M _⊙	2.34·10 ⁻¹	2.80·10 ⁻¹	2.14·10 ⁻³	4.76·10 ⁻²	5.82·10 ¹⁷	1.27·10 ¹⁸	4.99·10 ¹⁷	8.34·10 ¹⁶
LMP, 40M _⊙	1.71·10 ⁻¹	1.72·10 ⁻¹	6.44·10 ⁻³	7.23·10 ⁻³	4.25·10 ¹⁷	1.26·10 ¹⁸	4.10·10 ¹⁷	1.58·10 ¹⁶

NOTE.— F is the time-integrated central weak flow ($F_i \equiv \int_{t_{\text{O-dep}}}^{t_{\text{pre-SN}}} \lambda_{i,\text{central}}(t) dt$), and respectively F_{EC} , F_{β^+} , and F_{β^-} are the contributions due to electron capture, β^- -decay and β^+ -decay, $F = F_{\text{EC}} + F_{\beta^+} - F_{\beta^-}$. E_{weak} , E_{plas} , E_{EC} , and E_{β^-} are the total specific energy loss by neutrinos due to all weak interactions, plasma neutrinos, electron capture and β^- -decay.